Fabrication and characterization of $(Zn_{1-x}Mg_x)_3N_2$ thin films with different compositions

By

Sidra Shakoor

(134-FBAS/MSPHY/F12)

FACULTY OF BASIC AND APPLIED SCIENCES,

INTERNATIONAL ISLAMIC UNIVERSITY,

ISLAMABAD

(2015)

Accession No. TH17284

MS
620.5
SIF

Nanotechnology.
Magnesium.
Liquid phase epitaxy.
X-ray diffraction.

بسم الله الرحمن الرحيم

Fabrication and characterization of $(Zn_{1-x}Mg_x)_3N_2$ thin films with different compositions

Sidra Shakoor

(134-FBAS/MSPHY/F12)

Supervisor

Dr. Shaista Shahzada

Assistant Professor,

Department of Physics, FBAS, IIUI

Co-Supervisor

Dr. Arshad Mehmood Janjua

Deputy Chief Scientist

NILOP Islamabad

DEPARTMENT OF PHYSICS

FACULTY OF BASIC AND APPLIED SCIENCES,

INTERNATIONAL ISLAMIC UNIVERSITY, ISLAMABAD (2016)

INTERNATIONAL ISLAMIC UNIVERSITY, ISLAMABAD

FACULTY OF BASIC AND APPLIED SCIENCES

DEPARTMENT OF PHYSICS

Fabrication and characterization of $(Zn_{1-x}Mg_x)_3N_2$ thin films with different compositions

By: **Sidra Shakoor**

(Registration No. 134-FBAS/MSPHY/F12)

A thesis submitted to

Department of Physics

for the award of the degree of

MS Physics

Signature: ______________________________

Dr. Shumaila Sajjad

(Acting Chairperson, Department of Physics)

Signature: ______________________________

Dr. Muhammad Sher

(Dean FBAS, IIU, Islamabad)

INTERNATIONAL ISLAMIC UNIVERSITY, ISLAMABAD

FACULTY OF BASIC AND APPLIED SCIENCES

DEPARTMENT OF PHYSICS

Dated: 13th Feb., 2014.

FINAL APPROVAL

It is certified that the work presented in this thesis entitled "**FABRICATION AND CHARACTERIZATION OF $(Zn_{1-x}Mg_x)_3N_2$ THIN FILMS WITH DIFFERENT COMPOSITIONS**" by **Ms. Sidra Shakoor** bearing **Registration No. 134-FBAS/MSPHY/F12** is of sufficient standard in scope and quality for the award of degree of MS Physics from International Islamic University, Islamabad.

COMMITTEE

External Examiner

Dr. Muhammad Raffi

Deputy Chief Scientist,

NILOP Islamabad

Internal Examiner

Dr. Naeem Ahmad

Assistant Professor

Department of Physics, FBAS, IIUI

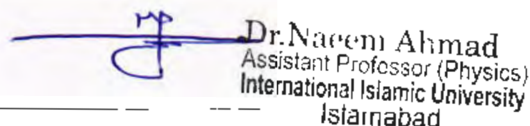

Supervisor

Dr. Shaista Shahzada

Assistant Professor,

Department of Physics, FBAS, IIUI

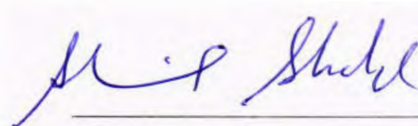

Co-supervisor

Dr. Arshad Mehmood Janjua

Deputy Chief Scientist,

NILOP Islamabad

A thesis submitted to

Department of Physics

International Islamic University Islamabad

as a partial fulfilment for the award of the degree of

MS in Physics

TO MY HUSBAND, FAMILY

AND TEACHERS

WHO SUPPORTED,

ENCOURAGED AND HELPED

ME IN ALL POSSIBLE WAYS

Acknowledgement

In the name of **Allah**, the Most Gracious and the Most Merciful Alhamdulillah, all praises to **Allah** for the strengths and **His** blessings in completing this thesis. I find absolutely no words to express my deepest appreciation to my beloved **Holy Prophet Muhammad (ﷺ)**, the fountain of knowledge and guidance for all worlds.

First of all, I offer my sincerest gratitude to my supervisor, **Dr. Shaista Shahzada** (Assistant Professor IIUI) who has supported me throughout my thesis with her patience, encouragment and knowledge whilst giving me the chance to work in my own way. One simply could not wish for a better or more affectionate supervisor.

I am especially thankful to **Dr. Mushtaq Ahmad** (Director NILOP) for allowing me to use all the apparatus and facilitated in every possibly way to fulfil the requirements of the research. Special appreciation goes to my co. supervisor, **Dr. Arshad Mehmood Janjua** (Deputy Chief Scientist NILOP) for his supervision and constant support. His invaluable help of constructive comments and suggestions throughout the experimental and results evaluation work have contributed to the success of this research. I am extremely grateful to **Mr. Bilal Mahmood** (Tech 1, Material Division, PINSTECH) for his selfless professional help and effort in target making. I would like to express my appreciation to **Qaisar Raza** (Principal Scientist NILOP). I always found him kind, supporting and helping. Also, **Amjad Iqbal** (Senior Scientist, NILOP) and **Shahid Mehmood** helped me a lot in setting the required apparatus.

I am also thankful to Sir **Tariq Jan,** Sir **Abdul Jabbar** and Miss **Asma Nazir** (Ph.D. scholars) at IIUI. They were always caring, kind and helping to me. I am highly obliged to **Dr. Ahmad Shuja Syed, Engineer Ali** and **Engineer Shoaib** of **Advanced Electronics Laboratory (AEL)** under IDB funded project IIUI for their utmost help in the characterization of my samples. They also aided me positively in the analysis as well as discussion of the results obtained by electrical as well as optical characterizations. They also encouraged us to observe how different characterizations were carried out on our samples.

I absolutely found no words to express my deepest feelings for my all loving family members, especially to my beloved husband **M. Anees Akhtar** and my **mother.** They are always passionate, kind, supportive and encouraging. They always prayed for me. Especially my husband provided me with his moral and financial support.

I am also thankful to my all friends especially to Anbarin Fatima and Saima Naz for their encouragement and every possible help during this research work. I am greatly grateful to **IIUI, NILOP** and **PIEAS** for providing me facilities to use their labs.

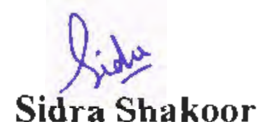

Sidra Shakoor

IIU, Islamabad

Table of Contents

List of figures.. (XI)

List of tables.. (XIV)

List of abbreviations.. (XV)

List of symbols.. (XVII)

Abstract... (XVIII)

1 Introduction..1

1.1 Nanotechnology...1

1.2 Materials..1

1.2.1 Zinc Nitride (Zn_3N_2)..2

1.2.2 Magnesium (Mg)..3

1.3 Thin Film..5

1.3.1 Thick and thin film...6

1.3.2 Brief History...6

1.3.3 Properties of thin film differ from bulk material..........................7

1.3.4 Film deposition and film formation...7

1.4 Applications...7

1.5 Characteristics to be studied..9

1.6 Deposition techniques..10

1.6.1 Ion implantation..11

1.6.2 Liquid Phase Epitaxy (LPE)..11

1.6.3 Chemical Vapour Deposition (CVD)...11

1.6.4 Pulsed Laser Deposition (PLD)..11

1.6.5 Atomic Layer Deposition (ALD)..12

1.6.6 Spray coating...12

1.6.7 Thermal evaporation...13

1.6.8 Sputtering..13

2 Experimental Setup......17

2.1 Preparation of target......17

2.2 Substrate selection......18

2.3 Vacuum pumps......18

2.4 Experimental details......19

2.5 Practical procedure......19

3 Characterization techniques to be used......22

3.1 X-Ray Diffraction (XRD)......22

3.2 Atomic Force Microscopy (AFM)......24

3.3 Raman Spectroscopy......25

3.4 Spectroscopic Ellipsometry (SE)......26

3.4.1 Principle of ellipsometry......27

3.5 Spectrophotometer......29

3.5.1 UV-VIS Reflectance Spectroscopy......29

3.6 Electrical Characterizations (IV measurements)......30

3.6.1 Sheet Resistance......30

4 Results and Analysis......33

4.1 Structural Analysis (XRD)......33

4.1.1 Sample no. 1 (Zinc Nitride $Zn_3N_2(x = 0)$)......33

4.1.2 Sample no. 2 ($(Zn_{1-x}Mg_x)_3N_2$ (x = 0.05))......35

4.1.3 Sample no. 3 ($(Zn_{1-x}Mg_x)_3N_2$ (x = 0.15))......37

4.1.4 Sample no. 4 ($(Zn_{1-x}Mg_x)_3N_2$ (x = 0.25))......38

4.1.5 Sample no. 5 ($(Zn_{1-x}Mg_x)_3N_2$ (x = 0.35))......40

4.2 Raman Spectroscopy......43

4.2.1 Zinc Nitride thin film (Zn_3N_2)......43

4.2.2 Zinc Magnesium Nitride thin film (ZnMg1 (95:05))......44

4.2.3 Zinc Magnesium Nitride thin film (ZnMg2 (85:15))......44

4.2.4 Zinc Magnesium Nitride thin film (ZnMg3 (75:25))………45
4.2.5 Zinc Magnesium Nitride thin film (ZnMg4 (65:35))………46
4.3 Electrical Characterizations……………………………………47
4.4 Optical Characterizations……………………………………...51
4.4.1 UV-VIS Reflectance Spectroscopy………………………...51
4.4.2 Spectroscopic Ellipsometry (SE)…………………………..57
4.5 Conclusions……..…………………………………………………62
5 References………………………………………………………64

List of Figures

Fig. 1.1: Crystal structure of Zn_3N_2.

Fig. 1.2: Crystal structure of magnesium.

Fig. 1.3: Thin film technology; materials and applications

Fig. 1.4: Thin Film Deposition Techniques.

Fig. 1.5: Pulsed Laser Deposition (PLD)

Fig. 1.6: Schematic diagram of ALD

Fig. 1.7: Schematic diagram of spray coating

Fig. 1.8: Schematic diagram of sputtering.

Fig. 2.1: Photograph of (a) Rotary Vacuum Pump, (b) Turbo-molecular Vacuum Pump.

Fig. 2.2: Photograph of Experimental Setup used.

Fig. 2.3: Schematic diagram of dc sputtering.

Fig. 2.4: Photograph of (a) Zinc target loaded in the chamber's target holder, (b) Plasma Generation.

Fig. 3.1: Schematic diagram of XRD system.

Fig. 3.2: Diagram showing Diffraction of X-rays.

Fig. 3.3: X-Ray Diffractometer.

Fig. 3.4: Schematic diagram of AFM.

Fig. 3.5: Raman Spectroscopy.

Fig. 3.6: Schematic diagram of Raman spectroscopy.

Fig. 3.7: A Typical Ellipsometer

Fig. 3.8: Schematic diagram of basic principle of SE

Fig. 3.9: Schematic diagram of a typical spectrophotometer.

Fig. 3.10: Four – point probing.

Fig. 4.1: X-ray diffraction pattern of Zn_3N_2.

Fig. 4.2: X-ray diffraction pattern of ZnMg1 (95:05).

Fig. 4.3: X-ray diffraction pattern of ZnMg2 (85:15).

Fig. 4.4: X-ray diffraction pattern of ZnMg3 (75:25).

Fig. 4.5: X-ray diffraction pattern of ZnMg4 (65:35).

Fig. 4.6: XRD patterns' comparison of $(Zn_{1-x}Mg_x)_3N_2$ with x = 0, 0.05, 0.15, 0.25 & 0.35.

Fig. 4.7: Raman spectra of Zinc nitride thin films (Zn_3N_2).

Fig. 4.8: Raman spectra for ZnMg1 (95:05).

Fig. 4.9: Raman spectra for thin film ZnMg2 (85:15).

Fig. 4.10: Raman spectra of ZnMg3 (75:25).

Fig. 4.11: Raman spectra for ZnMg4 (65:35).

Fig. 4.12: Comparison of $(Zn_{1-x}Mg_x)_3N_2$ with x = 0, 0.05, 0.15, 0.25 & 0.35.

Fig. 4.13: Graph of mobility (μ) of $(Zn_{1-x}Mg_x)_3N_2$ with x = 0, 0.05, 0.15, 0.25 & 0.35

Fig. 4.14: Graph of carrier concentration (N_s) of $(Zn_{1-x}Mg_x)_3N_2$ with x = 0, 0.05, 0.15, 0.25 & 0.35.

Fig. 4.15: Graph of sheet resistance (R_s) of $(Zn_{1-x}Mg_x)_3N_2$ with x = 0, 0.05, 0.15, 0.25 & 0.35.

Fig. 4.16: Comparison graph of mobility and carrier density of $(Zn_{1-x}Mg_x)_3N_2$ with x = 0, 0.05, 0.15, 0.25 & 0.35.

Fig. 4.17: IV curves of $(Zn_{1-x}Mg_x)_3N_2$ with x = 0, 0.05, 0.15, 0.25 & 0.35.

Fig. 4.18: Reflectance curve for $(Zn_{1-x}Mg_x)_3N_2$ (x = 0).

Fig. 4.19: Graph between hv and $(hv\ F(R))^2$ for ZnMg0$(Zn_{1-x}Mg_x)_3N_2$ (x = 0)..

Fig. 4.20: Graph between the wavelength and reflectance of $Zn_{1-x}Mg_x)_3N_2$ with x = 0. 0.05, 0.15, 0.25 & 0.35.

Fig. 4.21: Graph between hv and $(hv\alpha)^2$ for ZnMg1 (x = 0.05).

Fig. 4.22: Graph between hv and $(hv\alpha)^2$ for ZnMg2 (x = 0.15).

Fig. 4.23: Graph between hν and $(h\nu\alpha)^2$ for ZnMg3 (x = 0.25).

Fig. 4.24: Graph between hν and $(h\nu\alpha)^2$ for ZnMg4 (x = 0.35).

Fig. 4.25: Graph of refractive indices 'n' for $Zn_{1-x}Mg_x)_3N_2$ with x = 0, 0.05, 0.15, 0.25 & 0.35.

Fig. 4.26: Graph of extinction coefficient 'k' for $Zn_{1-x}Mg_x)_3N_2$ with x = 0, 0.05, 0.15, 0.25 & 0.35.

Fig. 4.27: Bandgap calculation of ZnMg0 (x = 0) by SE (using Tauc plot).

Fig. 4.28: Bandgap calculation of ZnMg1 (x = 0.05) by SE (using Tauc plot).

Fig. 4.29: Bandgap calculation of ZnMg2 (x = 0.15) by SE (using Tauc plot).

Fig. 4.30: Bandgap calculation of ZnMg3 (0.25) by SE (using Tauc plot).

Fig. 4.31: Bandgap calculation of ZnMg4 (x = 0.35) by SE (using Tauc plot).

List of Tables

Table 1.1: Classification of nanomaterials.

Table 4.1: Structural parameters of Zn_3N_2.

Table 4.2: Comparison of obtained and theoretical values of 'a'.

Table 4.3: Structural parameters of ZnMg1 (95:05).

Table 4.4: Structural parameters of ZnMg2 (85:15).

Table 4.5: ZnMg3 (75:25) 2θ values along with corresponding planes (hkl).

Table 4.6: Structural parameters of ZnMg3 (75:25).

Table 4.7: ZnMg4 (65:35) 2θ values along with corresponding planes (hkl).

Table 4.8: Structural parameters of ZnMg4 (65:35).

Table 4.9: Electrical values calculated by IV and 4-point probing.

Table 4.10: E_g values for different thin film samples.

Table 4.11: E_g values for different thin film samples calculated by SE.

Table 4.12: n & k values for different samples calculated by SE.

Table 4.13: Comparison of bandgap values calculated by UV-VIS reflectance and SE.

List of Abbreviations

QDs	Quantum Dots.
T_c	Conversion/working temperature of superconductor.
Zn_3N_2	Zinc Nitride.
Sc_2O_3	Scandium oxide.
CaF_2	Calcium Flouride.
ZnO:N	Nitrogen doped Zinc Oxide.
eV	Electron Volt.
nm	Nanometer.
GPa	Giga Pascal.
OLED	Organic Light Emitting Diode.
TFT	Thin Film Technology.
LCD	Liquid Crystal Display.
PVP	Physical Vapour Deposition.
CVD	Chemical Vapour Deposition.
LPE	Liquid Phase Epitaxy.
PLD	Pulsed Laser Deposition.
ALD	Atomic Layer Deposition.
DC	Direct Current.
RF	Radio Frequency.
PVA	Poly Vinyl Acetate.
AlN	Aluminium Nitrate
sccm	Standard Cubic Centimeters.
mbar	Milli Bars

Ar	Argon.
XRD	X-Ray Diffraction.
FWHM	Full Width at Half Maximum.
AFM	Atomic Force Microscope.
TEM	Tunnelling Electron Microscopy.
UV-VIS	Ultra Violet-Visible.
SE	Spectroscopic Ellipsometry.

List of Symbols

λ	Wavelength.
β	Full Width at Half Maximum.
Δ	Phase.
ω	Angular frequency.
Ψ	Amplitude.
n	Refractive index.
k	Extinction coefficient.
E_g	Bandgap.
ρ	Resistivity.
σ	Conductivity.
μ	Mobility.
Ω	Ohm (unit of Resistance).
α	Absorption coefficient.
ν	Frequency.
h	Plank's constant.

Abstract

Sputtering is a simple, well-controlled, reliable and one-step process for the fabrication of stable and good quality thin films. It provides a good physical control over the composition and hence properties of the fabricated thin films.

The thin films of zinc nitride (Zn_3N_2) and zinc magnesium nitride thin films have been fabricated using a pure Zn target and differently composed ZnMg targets prepared in weight ratio. A highly vacuumed deposition chamber is used with 50% N_2& 50% Ar gas introduced in the chamber. 1.5kW dc power is used and p-Si substrate is heated prior to deposition to 300°C for obtaining good quality thin films. The deposition time used is 1 hour. The crystallinity, lattice parameters and calculation of the grain size of thin films have been investigated by X-Ray Diffraction (XRD). The electrical behaviour of the fabricated thin films has been checked by I-V profiling of thin films. Optical properties were measured by UV-VIS reflectance, Raman spectroscopic and Spectroscopic Ellipsometry. The average calculated values of E_g calculated by reflectance and ellipsometry for thin films ZnMg0, ZnMg1, ZnMg2, ZnMg3 and ZnMg4 are 3.15, 2.9, 2.95, 3.35 and 3.25eV respectively. It is clear that the crystallinity of the thin films is decreasing with increase in Mg content.

1 Introduction

1.1 Nanotechnology:

Nanotechnology is one of the major scientific and engineering fields now a days as it unites knowledge from the fields of Physics, Chemistry, Biology, Engineering etc. It is an emerging technology with a wonderful ability to lead us to major breakthroughs that can be applied to facilitate the human life. The applications of nanomaterials in electronic and mechanical devices, in optical and magnetic elements, tissue development, and other biotechnologies are economically the most important and attractive features of nanotechnology.

Nanomaterials are classified according to their dimensions as stated in table 1.1.

No.	Classification	Dimension	Examples
1	Zero dimension	3-Dim.< 100 nm	QDs, nanoparticles etc.
2	One dimension	2-Dim.< 100 nm	Nano fibers, nanowires, nano rods, etc.
3	Two dimension	1_Dim.< 100 nm	Thin films, nano-thin coatings, etc.
4	Three dimension	All Dim.>100nm	Bulk Material.

Table 1.1: Classification of nanomaterials.

1.2 Materials:

Nitride semiconductors have been acknowledged as one of the most suitable material for optical as well as high-speed electronic devices (components) due to their properties like wide band gap value, greater electron saturation velocity and large breakdown voltage[1]. Up to now, transparent conductors and other such electrical components have been bound to oxide-based semiconducting materials. To look into

new materials for above transparent conductors with large refractive indices to ensure large transmission, we have to target the nitrides having wide band gaps as the polarizability of nitrogen is greater than oxygen[2]. However, the reports about nitrides belonging to group II are much lesser than group III nitrides[1]. Zinc nitride (Zn_3N_2) is selected among other group II nitrides as zinc has an attractive electronic structure than any other.

1.2.1 Zinc Nitride (Zn_3N_2):

Zinc nitrideis a compound semiconducting material (belonging to groups II-V).Zn_3N_2 powder was synthesized for the very first time by Juza and Hahn in 1940[3]. And it remained a relatively less studied material. Its color in powder shape is blackish. It has the anti-scandium oxide (Sc_2O_3) crystal structure i-e. a derivative of the CaF_2 structure, where nitrogen atoms occupy the calcium positions and zinc atoms occupy three-fourth of the fluorine atoms' positions[4](fig. 1.1).

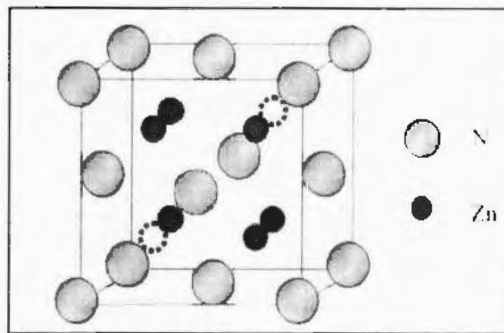

Fig. 1.1: Crystal structure of Zn_3N_2

This material has is significance as a new semiconductor material in photovoltaic, electronic, optoelectronic and other such devices. It has been the centre of research for few last years and its properties are found to differ depending upon the method of fabrication used. It can also be used as a starting material to obtain ZnO:N[5]. Preparing ZnO:N using zinc nitride as precursor (material to start with) offers a way to avoid some technical problems in direct doping of N in ZnO such as low solubility of Nitrogen in ZnO etc. But the reliability and reproducibility of the results is still debatable as the chemical activation level of O is higher than that of N. Hence, Zn is susceptible to combine with O rather than N[6].Zinc oxide exhibits dual properties of a semi-conductor and a piezoelectric material[7]. Also it is non-toxic, less expensive and found abundantly.

Several methods of fabrication have been used in literature for the development of zinc nitride films which include direct chemical synthesis[8], molten salt electrochemical method[1], reactive pulsed laser deposition[9], atomic layer deposition[10] but the most commonly used method is magnetron sputtering[2, 4, 5, 11-15]. Considerable challenges in fabrication of such thin films are still present, including the control and reproducibility of structural composition and electrical properties, stability of deposited thin films in ambient condition and especially the problem of unsought oxidation of the films[13]. In trials to comprehend the properties and basic parameters related to zinc nitride, significant disagreements have been reported on the values of some basic physical parameters, such as the energy band gap's type and value and the conductivity type. The energy band gap as per reporting ranges from 1.01eV to 3.2eV and it can either be direct or indirect band gap depending upon the technique used for depositing and characterizing Zn_3N_2[8, 12, 16, 17]. Both n-type and p-type zinc nitride, either in as-prepared and annealed forms were reported [4, 18, 19].

Applications: Zn_3N_2 has a potentiality as a new semiconducting material in electronic, optoelectronics, photovoltaics and sensor applications, along with some extra and important advantages such as eco-friendly processing, unlimited availability and lower fabrication cost[11].

1.2.2 Magnesium (Mg):

The name *magnesium* comes from the Greek word magnesia; a district in east Thessaly. It is related to magnetite and manganese, whose names also originated from the same area. It was discovered as a separate element by Joseph Black in 1735. It is a ductile shiny grey white metal with a hexagonal closed packed crystalline structure. Mg is the eight most exuberant elements in Earth's crust i.e. 2% of it. It is very reactive hence always found naturally in compound form only. It is blackened slightly when exposed to air but an oxygen-free environment is not required for its storage because magnesium is protected by a thin layer that is fairly damp-proof and difficult to remove.

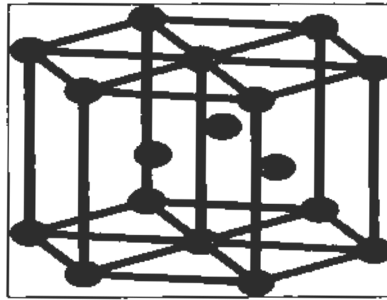

Fig. 1.2: Crystal structure of magnesium.

Some of its properties are as follows:

Physical properties:

Phase	Solid
Melting Point	923K (650^{0}C)
Boiling Point	1363K (1091^{0}C)
Density	1.738g/cm^3

Mechanical properties:

Tensile strength	220MPa
Yield strength	130MPa
Bulk/Elastic modulus	45GPa
Mohs Hardness	1-2.5
Shear modulus	17GPa

Chemical properties:

In air, it easily ignites and burns with a bright white flame.

Atomic Number	12
Ionic radius	0.065nm

Isotopes	5

Applications:

- Magnesium compounds are used mostly as refractive lining in furnaces for the production of metals, glass and cement.
- As it is very light, with a density i.e. two-third of that of aluminium's, it is used in reducing weights e.g. in aeroplanes, missiles, cameras, laptops, luggage carriers etc.
- It improves the mechanical, preparation and welding characteristics of aluminium used for alloying.
- Mg compounds are commonly used in fields like industry and agriculture.
- It also has vast applications in photography, printing industry, flares and pyrotechnics.
- It has a low toxicity.
- Another important use of Mg is that it is used an anti-corrosion agent for iron and steel in pipelines and ship bottoms.

In the present work, zinc nitride thin films are to be doped with magnesium for the purpose of engineering its band gap. Doping of zinc nitride thin films is to be done for the first time and band gap tailoring will help us greatly to achieve our goal of using zinc nitride thin films in electrical and opto-electrical devices accordingly.

1.3 Thin Film:

Every material's upper layer (i.e. its surface) is open to various natural phenomena. The surface of a solid body is prone to wear due to corrosion and has to interact with electromagnetic radiations as well as light. Also from technological point of view, the size reduction of mechanical, electrical, optical and optoelectronic components continuously adds to the surface to volume ratio of the material used. Hence, some of the surface related properties of the material become significantly important. So by keeping this in mind, films or coatings are commonly used to obtain the desired results in the manufactured component. For example, a mechanical component can be made with a high hardness (to prevent wear and tear) and a high fracture hardness (to avoid propagation of a crack) can be made by using a composite; a coating surface to provide high fracture toughness and a solid hard bulk core to

avoid wear and tear of the component. Another examples of thin films are anti-reflection coatings (used in photovoltaics), electromagnetic blocking coatings etc.

1.3.1 Thick and thin films:

The exact difference between 'thick' and 'thin' films cannot be generally defined as it is not pin pointed in literature. Basically, a film can be conceived as a thin film if its overall properties differ from those of the bulk material. This can happen either due to the increasing surface to volume ratio or by dependence of themicroscopic structure on the deposition parameters used.

1.3.2 Brief History:

In the following a short history of thin film technology is given on the bahalf of integrity:

1650: Observation and understanding of interference patterns (e. g. oil on water) by R.Boyle, R.Hooke, I.Newton.

1850: Elaboration of first deposition techniques (M.Faraday, W. Grove, T. A. Edison) and methods of thin film's thickness calculations (Arago, Fizeau, Wernicke, Wiener).

1940: Industrial fabrication of thin film coatings for optical, electronic and mechanical purposes (mostly military).

1965: Thin film technology becomes an intrinsic part of the manufacturing processes (on large scales) in semiconductor and optical industry.

1990: Thin films of Superconductors having high value of T_c.

1995: Thin film processing permits the engineering of microstructures having atomic and mesoscopic dimensions.

2000: Fabrication of nano-crystalline materials with desired crystal structure and composition for applications as protective coatings. Deposition of two as well as three dimensional objects with sizes in the nm range having a desired order perfection.

2004: Advancement of intricate reactive coating methods for industrial applications (coatings on glass as well as thermal management etc.).

2006: Exploration of organic materials' coatings gives rise to the invention of organic electronic components (OLED, printable circuits)[20].

1.3.3 Properties of thin films differ from the bulk materials:

The properties of a thin film that may differ from the bulk material are given below.

- Not fully dense
- Stresses are present
- Different defect structure from bulk
- Semi - two dimensional (i.e. extremely thin films)
- Strongly affected by surface and interface properties

1.3.4 Film Deposition and Film Formation:

The process used for the deposition or synthesis of a film can be divided into three basic steps.

1. Emission of particles from source (using heat, high voltage etc).
2. Transferring particles to substrate (base material for thin film).
3. Condensation or deposition of particles on substrate.

The deposition process used and/or the choice of the deposition parameters used conclude that either above steps will be independent or having a less or more influence on one another. The former is preferable as it allows the independent control of the basic steps hence providing a greater flexibility in the thin film deposition process.

General characteristics of thin film deposition includes deposition rate, film uniformity, material and substrate selection, quality of the deposited films, cost etc.

1.4 Applications:

There are wide number of applications and uses of thin films in almost every field of life. Some of which are as follows.

Engineering/processing:

It is used in fabricating protective coatings to minimize wearing out, corrosion and abrasion of the mechanical parts of machine (low friction coatings). Also to

make hard coatings for cutting tools. It is also used for surface passivation. It also provides protection against high temperature corrosion and methods to make self-supporting coatings of refractory metals for rocket tips, crucibles (melting pots, vessels), pipes etc. It can also be utilized in making decorative coatings.

Optics:

In Optics, thin film technology can be utilized for making anti-reflex coatings, highly reflecting coatings (laser mirrors), beam splitters and light polarizers. It also has several applications in integrated optics.

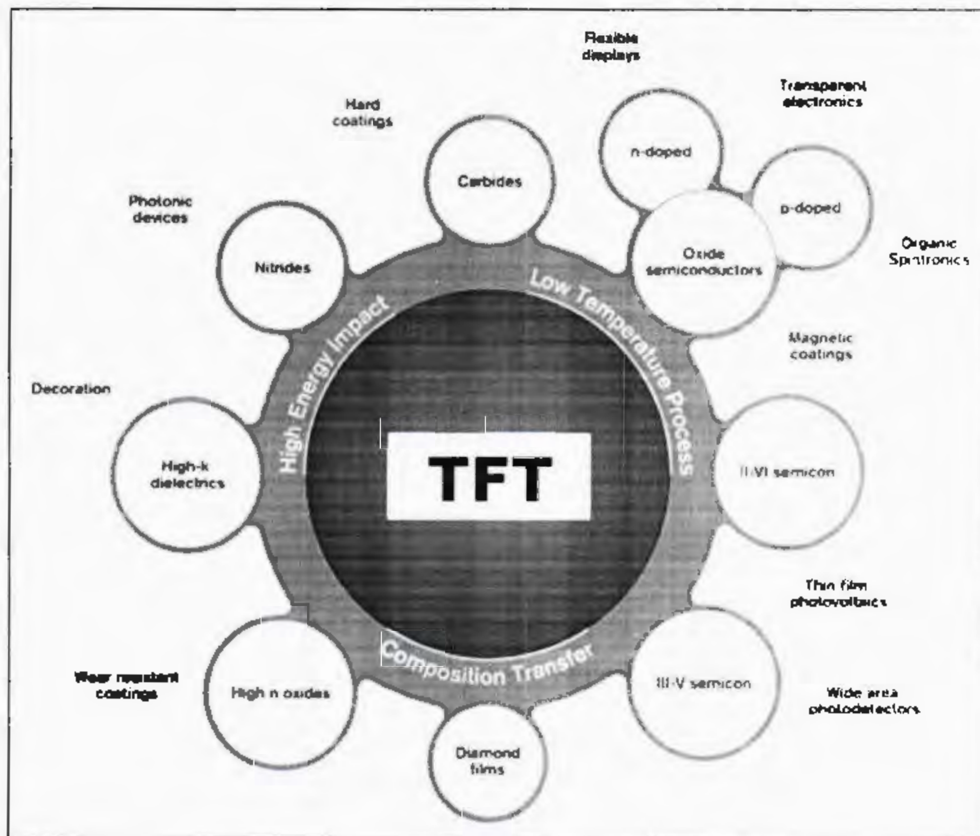

Fig. 1.3: Thin film technology; materials and applications

Optoelectronics:

It is utilized in photodetectors, image transmission as well as construction of LCD/LED/TFT.

Electronics:

It is successfully applied in making passive and active thin film elements (resistors and diodes) in circuitry, integrated circuits as well as anti-static coatings.

Magnetic applications:

Thin film technology is also applied in making audio, video and computer data storage devices also in read/write heads.

1.5 Characteristics to be studied:

- Morphology

  The characteristics to be studied related to the morphology contains microstructure, surface topology, crystalline structure, defect density, crystalline orientation etc.

- Chemical

  The chemical characteristics include the composition, impurities. reactivity, etching rate, stability, corrosion and erosion resistance etc.

- Electrical

  The electrical parameters that can be observed and studied contains resistivity, conductivity, dielectric constant, permittivity, radiation hardness etc.

- Thermal

  It includes coefficient of expansion, thermal conductivity, temperature dependence of all the related properties, volatility etc.

- Mechanical

  It contains information about fracture hardness, density, adhesion. anisotropy, elasticity, stresses and strains involved in the thin films.

- Optical

  It includes the observation and calculation of the refractive index, extinction coefficient, transmission, absorption and dispersion and reflectance spectra as well.

- Magnetic

  It includes the estimation of coercivity, permeability and saturation flux density.

1.6 Deposition Techniques:

There are two major groups of thin film deposition techniques as given below

1. Chemical Vapour Deposition (CVD) :

With reactant gases introduced in the chamber at high or low temperature, chemical reaction takes place of a volatile material giving rise to the deposition of a solid film (thick or thin) on a suitably placed substrate. This is called CVD. E. g. low pressure CVD (LPCVD), laser enhanced CVD (LECVD), plasma enhanced CVD (PECVD), sol-gel etc.

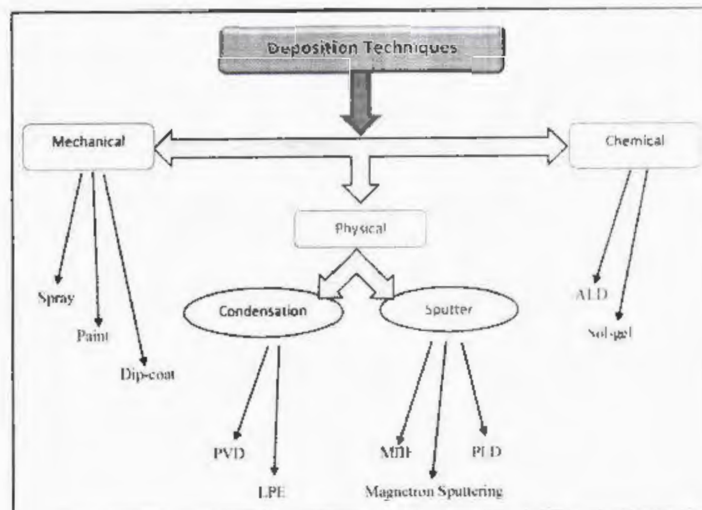

Fig. 1.4: Thin Film Deposition Techniques.

2. Physical Vapour Deposition (PVD):

Inside a chamber (mostly a vacuum chamber), vapours of the desired material are created which condenses on a substrate to give solid film. This is called PVD. E. g. evaporation, sputter deposition, pulsed laser deposition (PLD) etc.

There are also other methods which are widely in use now a days such as spin coating, electro-deposition, spray coating etc. Some of the common deposition techniques are briefly described in the next few paragraphs.

1.6.1 Ion implantation:

It is the process of planting or embedding energetic ions into the substrate by using electric fields to accelerate them. These ions are bombarded in the form of a beam. This technique is most commonly used for doping purposes.

1.6.2 Liquid Phase Epitaxy (LPE):

The word epitaxy means growth of monocrystalline structures and by epitaxial growth, we mean growth of structures which are different from deposited ones i.e. not polycrystalline or amorphous. Liquid phase epitaxy produces a thin monocrystalline film of compound semiconductors from their melt (similar to Czochralski technique)[21]. These films are deposited on a suitably selected single crystal substrate. It has some disadvantages as compared to Molecular Beam Epitaxy (MBE) like poor uniformity, bad surface morphology etc.

1.6.3 Chemical Vapour Deposition (CVD):

In CVD, components of the source; composed of material to be deposited, are vaporized. These vapours go through a chemical reaction with introduced gases near or on the substrate surface. After this, they are solidified at the substrate leading to a thin film[22]. Low temperature deposition normally produces amorphous films. For obtaining high-quality poly- or single-crystalline films high temperature processing is required.

1.6.4 Pulsed Laser Deposition (PLD):

This deposition technique makes use of laser to ablate/erode or remove the material to be deposited. Thin films are fabricated by the ablation of one or more target materials by focussing a pulsed-laser beam on them[23] Different types of laser can be used for this purpose depending on the desired outcome and feasibility. Mostly Nd:YAG laser is used for this purpose which is a solid state laser. Nd:YAG stands for Neodyium doped Yttrium Aluminium Garnet. YAG has gained more importance than other similar materials due to its suitable optical, thermal as well as mechanical properties to bear the severe operating conditions[24].

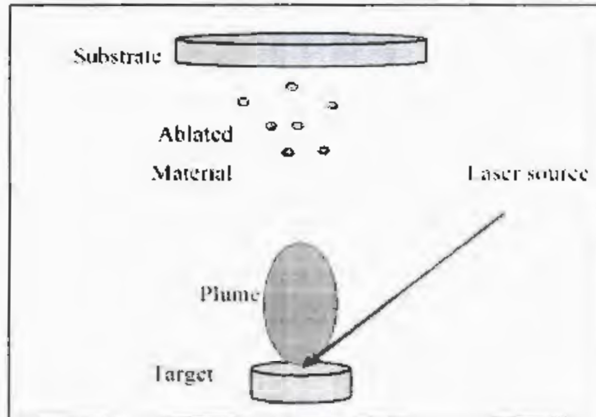

Fig. 1.5: Pulsed Laser Deposition (PLD)

1.6.5 Atomic Layer Deposition (ALD):

ALD is a deposition process in which the substrate is exposed to alternate gaseous species (normally named as precursors) to grow thin film. In contrast to CVD, its precursors are not present in the chamber simultaneously, instead they are introduced in a sequential series in the form of non-overlapping pulses. Precursor gases introduced on to the substrate surface will chemisorb or surface reaction takes place at the substrate. Surface reactions on ALD are self-limiting. Precursors used in ALD are preferably volatile liquid or gases[25].

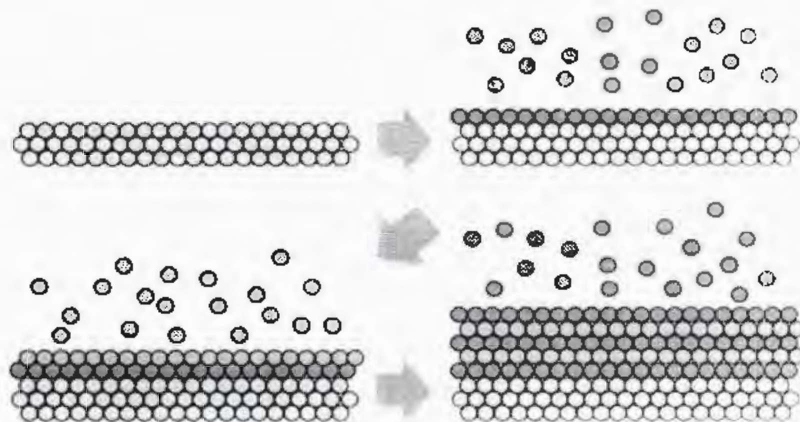
Fig. 1.6: Schematic diagram of ALD

1.6.6 Spray Coating:

In this deposition technique, a colloidal solution of the material to be deposited in any suitable solvent is sprayed on the substrate. Then it is left in

air for some time to dry and a thin film is created on the substrate. A proper weight ratio of solvent and solute is required for a good quality film production.

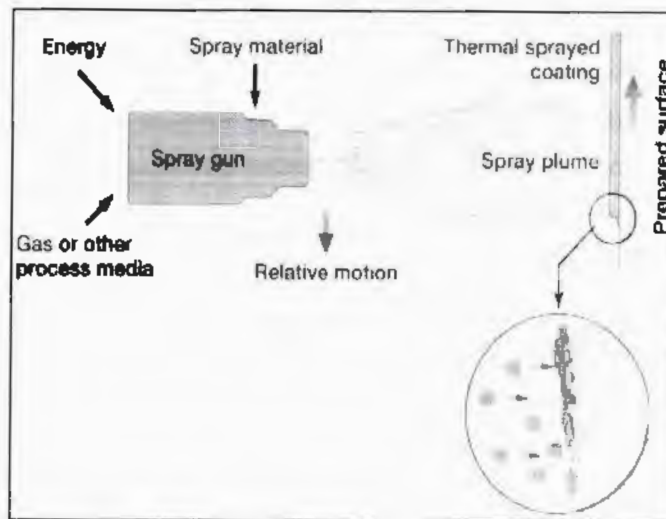

Fig. 1.7: Schematic diagram of spray coating

1.6.7 Thermal Evaporation:

It is a widely used technique for coating glass or polymer surfaces with thin metal layerse.g. aluminium coatings extensively used for making capacitors, as plastic wrappings, and as an obstructeragainst water diffusion. It is concerned with two basic steps: a hot source material evaporates (sublimation) and solidifies and accumulates on the substrate. It corresponds the well-known process by whichwater emerges on the lid of a boiling pot. The source material is vaporized in a vacuum which allows vapour particles to move directly to the substrate, where they solidify again[26].

1.6.8 Sputtering:

Sputtering is a thin film fabrication technique in which atoms are ejected from a surface when it is struck by sufficiently energetic particles (ions, atoms etc.). The basic working principle of sputtering is the transfer of momentum through physical collision just like the collisions of balls in billiard game. It is an alternate method to evaporation and used for depositing materials which are not easy to evaporate thermally. This technique was first

discovered in 1852, and it later developed as a thin film fabrication technique by Langmuir in 1920. Sputtering processes is basically divided into four types:

- DC
- RF
- Magnetron
- Reactive

Steps involved in sputter deposition are as follows:

1. Ions are produced and oriented towards a target.
2. The ions erodes target's atoms.
3. The ejected atoms are transferred to the substrate.
4. Atoms solidify and form a thin film on the substrate.

Reasons for using sputtering:

The reasons behind using sputtering are many but a few are discussed here; it has offers many benefits such as low growth temperature, good adherenceof thin films on substrate, large deposition rate and ability to form compound thin films using metallic targets. It also provides a chance to obtain c-axis oriented thin films. It allows the deposition of the target material without any chemical or compositional change. It can be used to produce economically feasible large area thin films with desired composition and properties[27]. Another advantage is the availability of different growth ambient[28]. It also offers to obtain thin films with high packing density[29]. Most of all in sputtering, by controlling different parameters such as vacuum pressure, substrate temperature, deposition time, gas flow rate and applied dc/rf power; we can manipulate the properties of the thin film grown. This is the main advantage of using a PVD as in CVD a person has no control over the composition and properties such as thickness of the thin films.

The key difference between magnetron sputtering as a plasma process and thermally excited thin film fabrication methods (evaporation, CVD) is the much higher energy input that can be obtained by magnetron sputtering[30].

As the targets used by me were metallic, hence ***DC sputtering*** is given in detail. In this process, the metallic/dielectric target is grounded and behaves like a cathode i.e. it is attached to cathode of the applied DC source. Chamber is vacuumed to ensure no particulates and purity of thin films. Argon gas is introduced in it. It provides high purity due to its inertness. The substrate on which films are to be deposited are placed on a platform connected to the anode of the DC supply. Electrons are accelerated between the cathode and anode which on colliding with the Ar gas, ionizes it and creates plasma. The positively charged ions are then directed towards the target where they sputter a large number of target atoms which are then deposited on the substrate.

Applications of Sputtering: Here are some common applications of the sputter deposition technique[33].

- Thin film deposition: It is usually done for future use in microelectronics, as a decorative coating on objects and also as a protective coating for safety of machine parts from wear and tear.
- Etching of targets: It includes the patterning of microelectronic devices as well as depth profiling microanalysis.
- Surface treatment: It can also be used for hardening of machine parts or any other thing and also for corrosion treatment.

2. Experimental Setup

2.1 Preparation of target:

Manual grinding of zinc and magnesium (both 99.999% pure) granules was carried out by using a mortar pestle in required weight ratios. The grinding equipment was cleaned with ethanol using an optical tissue to avoid any contamination. After cleaning the equipment, zinc was placed in it and was ground carefully by adding ethanol drop by drop in regular intervals to obtain fine powder. Grinding of zinc powder (in required weight ratios) was done for six hours at room temperature separately for each target. After getting powdered zinc, it was stored in a thoroughly clean bottle (cleaned using acetone). Same procedure was utilized for the grinding of Mg powder. After grinding, Zn and Mg were weighed in a physical balance at IIUI lab. After weighing the materials in required weight ratios, the powders were calcined at 250°C for 2 hours and pellets were made by using KOMAGE hydraulic press. One pellet of 2" diameter of pure zinc (ZnMg0) was made. Four composite pellets (2" diameter each) of ZnMg (95:05) (ZnMg1), ZnMg (85:15) (ZnMg2), ZnMg (75:25) (ZnMg3) and ZnMg (65:35) (ZnMg4) of Zn and Mg were also prepared in bracketed weight ratios. For this purpose, Zn and Mg finely ground powders were mixed evenly in mortar pestle in different selected weight ratios. The pressure applied for compressing powders into these pellets was 3 Ton. In ZnMg0, the mass of Zn used was 28.92g. In ZnMg1, mass of Zn was 27.47g and mass of Mg was 1.45g. ZnMg2, ZnMg3 and ZnMg4 were also made similarly in bracketed weight ratios such that whole mass remained 28.93 g required for a 2" diameter pellet. In ZnMg2, the mass of Zn was 24.58 gram and that of Mg was 2.89 gram. In ZnMg3, the mass of Zn was 21.69 g and mass of Mg was 7.23 g and in ZnMg4, the masses of Zn and Mg used were 18.8 g and 10.12 g respectively. As for making pellets with such a large diameter, compaction of very fine powders was a difficult task, we had to use a binder i.e. Poly Vinyl Acetate (PVA) in liquid form. Next step was the sintering of the compacted pellets to attain hardness as well as removal of the binder. A furnace was utilized for the purpose of sintering of these pellets. The temperature inside the furnace was raised from room temperature to 350°C and maintained at that temperature for 2 hours.

discovered in 1852, and it later developed as a thin film fabrication technique by Langmuir in 1920. Sputtering processes is basically divided into four types:

- DC
- RF
- Magnetron
- Reactive

Steps involved in sputter deposition are as follows:

1. Ions are produced and oriented towards a target.
2. The ions erodes target's atoms.
3. The ejected atoms are transferred to the substrate.
4. Atoms solidify and form a thin film on the substrate.

Reasons for using sputtering:

The reasons behind using sputtering are many but a few are discussed here; it has offers many benefits such as low growth temperature, good adherenceof thin films on substrate, large deposition rate and ability to form compound thin films using metallic targets. It also provides a chance to obtain c-axis oriented thin films. It allows the deposition of the target material without any chemical or compositional change. It can be used to produce economically feasible large area thin films with desired composition and properties[27]. Another advantage is the availability of different growth ambient[28]. It also offers to obtain thin films with high packing density[29]. Most of all in sputtering, by controlling different parameters such as vacuum pressure, substrate temperature, deposition time, gas flow rate and applied dc/rf power; we can manipulate the properties of the thin film grown. This is the main advantage of using a PVD as in CVD a person has no control over the composition and properties such as thickness of the thin films.

The key difference between magnetron sputtering as a plasma process and thermally excited thin film fabrication methods (evaporation, CVD) is the much higher energy input that can be obtained by magnetron sputtering[30].

Difference between RF and DC sputtering

Either RF or DC sputtering is to be used, it depends on the type of target used. If the target is metallic i.e. a conductor, a constant dc voltage can be used to accelerate the ions to desired bombarding velocity to sputter the target. On striking the surface of target, the resulting charge would be able to move freely on conducting target material resulting in no net charge accumulation on the target surface. But if the target material is an insulator, it will not allow such free movement of charges. On hitting the surface, the charge of ions will remain localized. With the passage of time, the charge will build up on the target making further bombardment of the surface impossible due to electrostatic repulsion. To prevent such problem, AC is utilized at a frequency above 50kHz. Such a high frequency is used to make sure only electrons can hit the target surface to neutralize the built up charge as heavy ions cannot follow such fast switching. This is called RF sputtering[31].

In *magnetron sputtering*, magnets are used to keep the ions confined in the region near the target surface enabling them to keep the plasma going. As it is clear from its name, *reactive sputtering* means there are some gases introduced in the chamber to enable the sputtered species to react with them and then get deposited on the substrate[22].

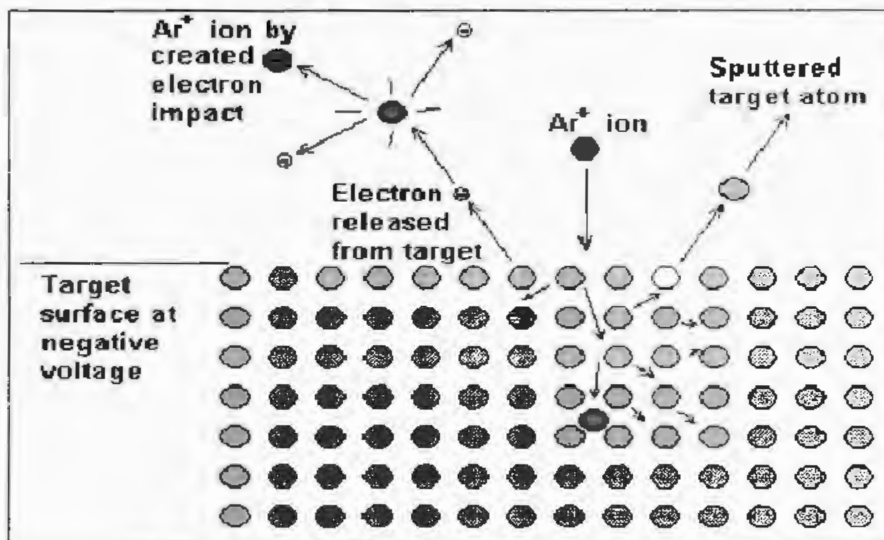

Fig. 1.8: Schematic diagram of sputtering[32].

As the targets used by me were metallic, hence ***DC sputtering*** is given in detail. In this process, the metallic/dielectric target is grounded and behaves like a cathode i.e. it is attached to cathode of the applied DC source. Chamber is vacuumed to ensure no particulates and purity of thin films. Argon gas is introduced in it. It provides high purity due to its inertness. The substrate on which films are to be deposited are placed on a platform connected to the anode of the DC supply. Electrons are accelerated between the cathode and anode which on colliding with the Ar gas, ionizes it and creates plasma. The positively charged ions are then directed towards the target where they sputter a large number of target atoms which are then deposited on the substrate.

Applications of Sputtering: Here are some common applications of the sputter deposition technique[33].

- Thin film deposition: It is usually done for future use in microelectronics, as a decorative coating on objects and also as a protective coating for safety of machine parts from wear and tear.
- Etching of targets: It includes the patterning of microelectronic devices as well as depth profiling microanalysis.
- Surface treatment: It can also be used for hardening of machine parts or any other thing and also for corrosion treatment.

2. Experimental Setup

2.1 Preparation of target:

Manual grinding of zinc and magnesium (both 99.999% pure) granules was carried out by using a mortar pestle in required weight ratios. The grinding equipment was cleaned with ethanol using an optical tissue to avoid any contamination. After cleaning the equipment, zinc was placed in it and was ground carefully by adding ethanol drop by drop in regular intervals to obtain fine powder. Grinding of zinc powder (in required weight ratios) was done for six hours at room temperature separately for each target. After getting powdered zinc, it was stored in a thoroughly clean bottle (cleaned using acetone). Same procedure was utilized for the grinding of Mg powder. After grinding, Zn and Mg were weighed in a physical balance at IIUI lab. After weighing the materials in required weight ratios, the powders were calcined at 250°C for 2 hours and pellets were made by using KOMAGE hydraulic press. One pellet of 2" diameter of pure zinc (ZnMg0) was made. Four composite pellets (2" diameter each) of ZnMg (95:05) (ZnMg1), ZnMg (85:15) (ZnMg2), ZnMg (75:25) (ZnMg3) and ZnMg (65:35) (ZnMg4) of Zn and Mg were also prepared in bracketed weight ratios. For this purpose, Zn and Mg finely ground powders were mixed evenly in mortar pestle in different selected weight ratios. The pressure applied for compressing powders into these pellets was 3 Ton. In ZnMg0, the mass of Zn used was 28.92g. In ZnMg1, mass of Zn was 27.47g and mass of Mg was 1.45g. ZnMg2, ZnMg3 and ZnMg4 were also made similarly in bracketed weight ratios such that whole mass remained 28.93 g required for a 2" diameter pellet. In ZnMg2, the mass of Zn was 24.58 gram and that of Mg was 2.89 gram. In ZnMg3, the mass of Zn was 21.69 g and mass of Mg was 7.23 g and in ZnMg4, the masses of Zn and Mg used were 18.8 g and 10.12 g respectively. As for making pellets with such a large diameter, compaction of very fine powders was a difficult task, we had to use a binder i.e. Poly Vinyl Acetate (PVA) in liquid form. Next step was the sintering of the compacted pellets to attain hardness as well as removal of the binder. A furnace was utilized for the purpose of sintering of these pellets. The temperature inside the furnace was raised from room temperature to 350°C and maintained at that temperature for 2 hours.

2.2 Substrate Selection:

Next step after target preparation was to select a suitable substrate. There are many different materials which are used as substrate material for growing thin film such as glass, sapphire, polymers, silicon etc. Polymeric substrates like polyethylene-terephthalate (PET), polycarbonate (PC), as polyphthalamide (PPA) are drawing attention of researchers probably due to their light weight, less cost and flexibility[34]. The substrate selected by us were such that it can withstand high growth temperature which is required for giving a thin film with a uniform thickness. In this work, p-type silicon (p-Si) substrate was used because it is relatively cheaper than other single crystalline substrate materials (like sapphire, AlN etc.). Large sized single crystal of Si are easily available at economical price and it can be cut to any desired size. Most of all, it is highly recommendable to integrate semiconductor thin films with Si substrates[30]. Another purpose of using p-Si substrate is to avoid large lattice mismatch between the thin films and its substrate.

Substrates were neatly cut using a diamond cutter with $1cm^2$ area of each. They were then sonicated in distilled water for 15 minutes then dried and cleaned using an optical tissue.

2.3 Vacuum Pumps:

Vacuum in the deposition chamber is attained in order to ensure the purity of the fabricated thin films. For this purpose, rotary vacuum pump (Ley Bold Heraeus type no. d16A) was used for attaining a rough or low vacuum ($\sim 10^{-3}$mbar) in the chamber; this is called *roughing.* Turbo-molecular pumps are momentum transfer pumps which use high speed fans to push and eject the gas atoms/molecules.

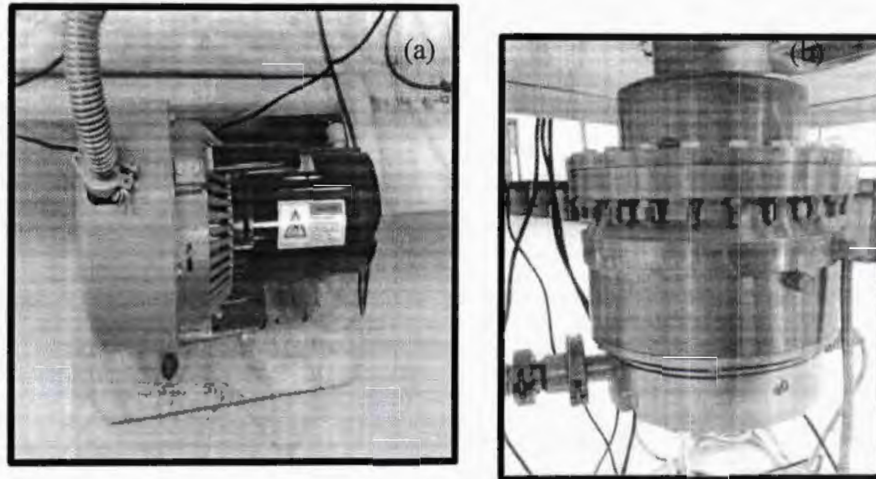

Fig. 2.1: Photograph of (a) Rotary Vacuum Pump, (b) Turbo-molecular vacuum Pump.

Fig. 2.1 shows the photographs of the vacuum pumps used in the present work. A turbo-molecular pump sweeps out a large area than a mechanical pump and does so frequently so it is capable of attaining much higher pumping speeds. Scroll pump (BLUFFTON try model no. 12010064080 was used to play a supporting role to maintain a specified pressure at the exhaust of the VARIAN turbo-molecular pump model no. 9698932 to create high vacuum (~10^{-6}mbar). This supporting function is called *backing*. If backing pump is not used, even a small pressure at the exhaust of the turbo-molecular pump can cause back streaming through the pump due to absence of a seal; this is called *stall*. To avoid it, a combination of turbo-molecular pump and scroll pump are used. Momentum transfer umps in combination with one/two positive displacement pumps gives the most commonly used configuration to achieve high vacuum.

2.4 Experimental Details:

All experiments were performed in the Thin Film Fabrication lab of National Institute of Laser and Optics (NILOP). The photograph of the experimental set up used is shown in fig. 2.2.

2.5 Practical Procedure:

DC reactive sputtering is one of the most desirable techniques for depositing nitride thin films as it can give high quality thin films even at low processing temperature. This technique can be used for all such applications where low

processing temperatures are most suited, hydrogen content of the films should be least and the composition of the films should be well under control. In particular, dc reactive sputtering is suited, because it facilitates by giving high deposition rates and is an industrial technique well suited for application on large areas as compared to other PVD technique.

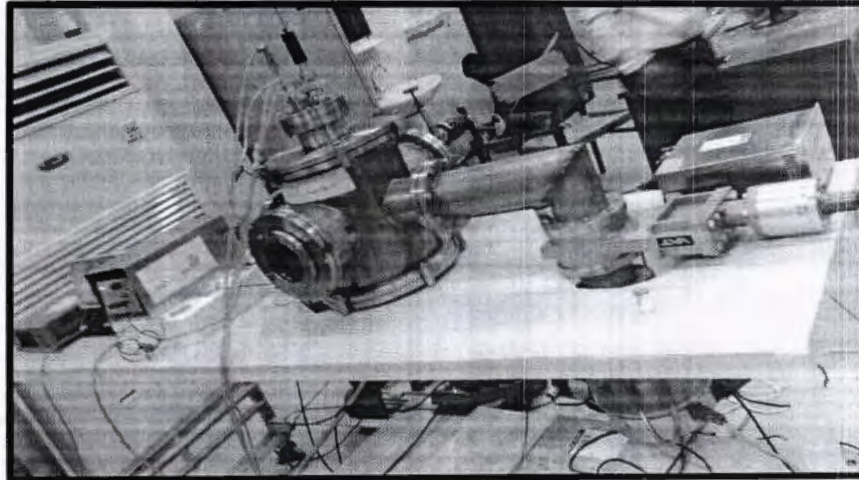

Fig. 2.2: Photograph of Experimental Setup used.

The apparatus used in this work contains following components:

1. Deposition chamber.
2. DC power supply (1.5kV).

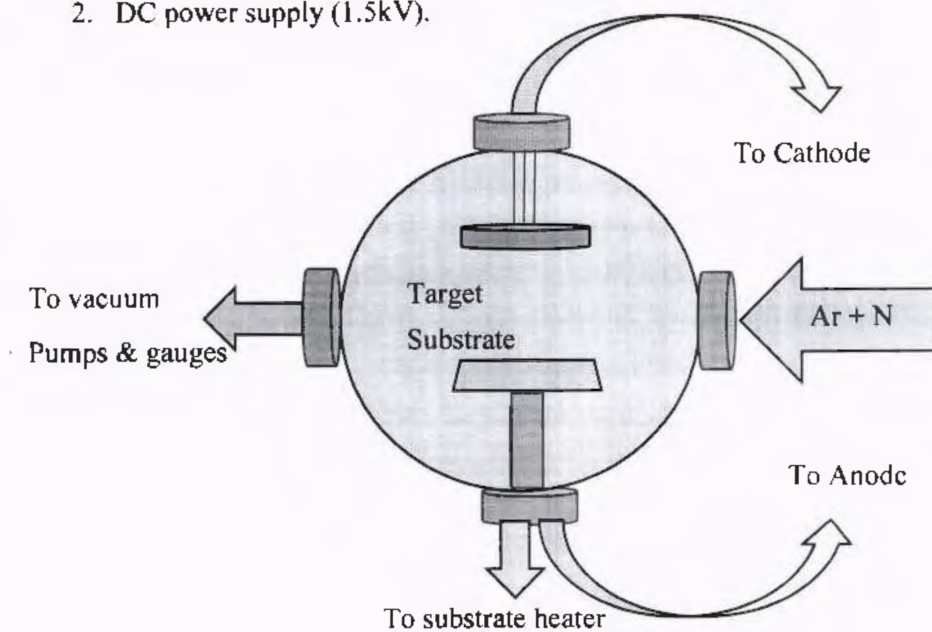

Fig. 2.3: Schematic diagram of dc sputtering

1. Gas mass flow controller.
2. Vacuum gauges for pressure measurements.
3. Vacuum pumps (rotary, scroll and turbo-molecular pumps).

Target of 2" (5.08cm) diameter was loaded in the apparatus. p-type Si substrates as prepared by above mentioned process were placed suitably on the substrate holding stage. The chamber was then closed and tightly fitted using O-rings and clamps. Rotary pump was used for attaining rough vacuum ~ 10^{-3}mbar. Then scroll pump was used for backing the turbo-molecular pump and a vacuum ~ 10^{-6}mbar was attained. Electric heater was used to fix the substrate at a temperature of 300^0C to ensure uniform thickness of thin film. Gases through mass flow controller were introduced with total regulated flow rate of 20sccm (standard cubic centimeter). 50% of N_2 (99.9999% pure) was introduced in the total flow of 20sccm. Water flow through pipes was regulated to keep the apparatus cool after plasma generation.

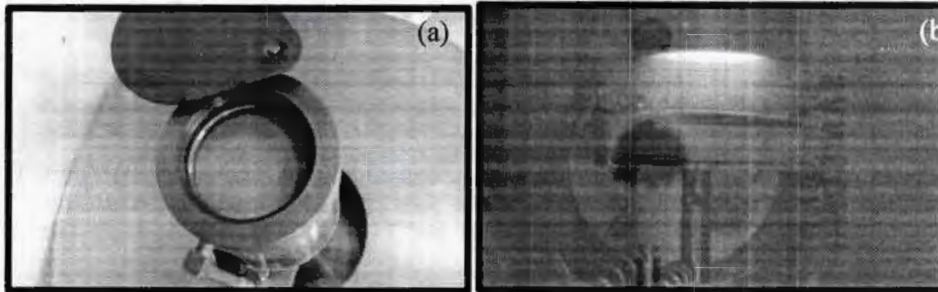

Fig. 2.4: Photograph of (a) Zinc target loaded in the chamber's target holder, (b) Plasma Generation.

Ar was used as inert gas for plasma generation. High-vacuum valve was configured in a way to generate plasma. .

Deposition was carried out for one hour at a pressure of 10^{-3}-10^{-4}mbar. After the chamber cooled down, it was opened and the samples were taken out and contained in sample boxes. Similar procedure was carried out with all the targets with same deposition parameters.

3. Characterization Techniques

There are some characterizations to be carried out in order to determine the structural, optical and electrical properties of the deposited thin films. These characterizations techniques along with a brief detail of each are discussed below:

3.1 X-Ray Diffraction (XRD):

X-ray diffraction (XRD) is a non-destructive technique which gives information about the crystallographic structure, phase identification, atomic spacing and chemical composition of the material. It provides information about the inter-planer distance and also the lattice parameters. X-ray diffraction pattern is different for different materials and it is a characteristic of a material. In a mixture of materials, a specific material's presence can be identified by its unique XRD pattern. It behaves same for a material as finger prints do for humans[26].

X-ray diffractometer consists of three main parts. These are X-ray tube, Sample holder and diffracted X-rays detector. A filament is heated inside a cathode ray tube; as a result of which electrons are ejected from it. These electrons are sped up towards the target used for x-rays generation by means of the applied voltage. When these moving electrons impinge the target, those having enough energy will knockout the electrons from the inner shells, resulting in the formation of X-rays. These X-rays are collimated and directed towards the sample by using necessary optics. These x-rays are scattered by the

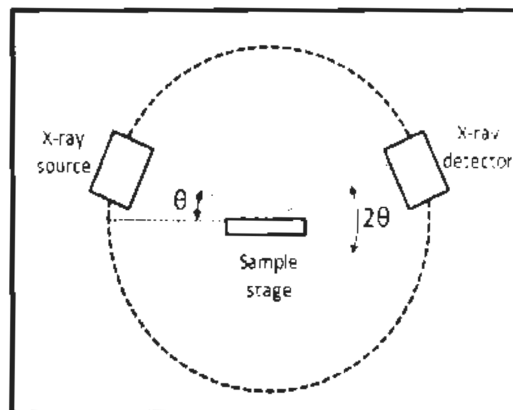

Fig.3.1: Schematic diagram of XRD.

atoms/planes of that material in all possible directions. The intensity of X-rays is recorded by rotation of the sample and detector. High intensity peaks recorded means constructive interference of the diffracted x-rays occurred and low intensities mean destructive interference happened there. Constructive interference occurs when the incident X-rays overlap on being diffracted by the sample and Bragg's law is satisfied. Bragg's law is given by the following equation

$$2d \sin\theta = n \lambda \ldots\ldots\ldots\ldots (3.1)$$

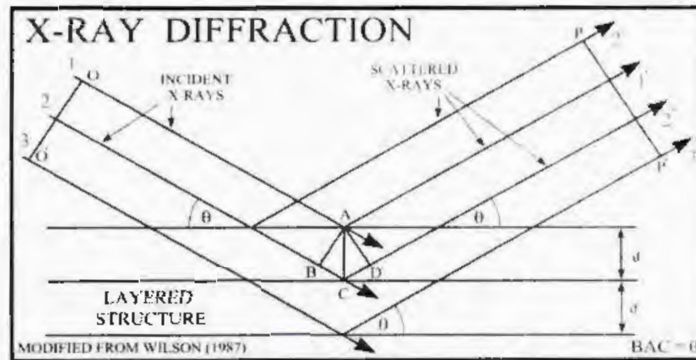

Fig. 3.2: Diffraction of X-rays.

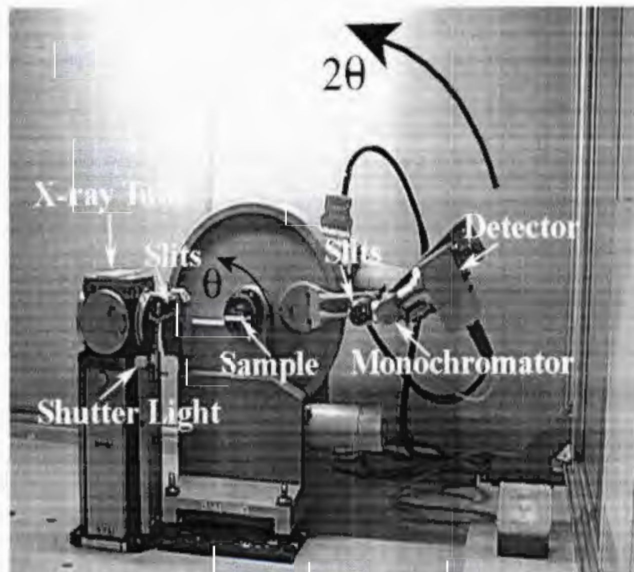

Fig. 3.3: X-Ray Diffractometer.

Where λ, n, d, θ are the wavelength of the x-rays, order of diffraction, inter-planar distance and angle of incidence respectively. The X-ray signal after being diffracted from the sample is further recorded and processed by an x-ray detector.

The mathematical relationship between inter-planar distance (d) and the miller indices (hkl) of the crystal structure is given by

For cubic,

$$\frac{1}{d^2} = \frac{h^2+k^2+l^2}{a^2} \ldots\ldots (3.2)$$

Here a, b and c are the lattice constants. The grain size is calculated by Full Width at Half Maximum (FWHM) of different X-ray graph peaks, by the use of Debye Scherer formula:

$$D= \frac{K\lambda}{\beta cos\theta} \ldots\ldots\ldots\ldots\ldots (3.3)$$

Here k is a constant, its value is 0.9, λ = 0.1540 nm is the wavelength and β is the full width at half maximum, it should be measured in degrees and then converted into radians for further calculations. θ is the angle of diffraction of the strongest peak[35].

The instrument used in the present study was x-ray diffractrometer, D8-Discover HR XRD (Bruker axes, Germany), using CuKα (λ=0.154 nm) in 2θ range which equals 10°-90°.

3.2 Atomic Force Microscopy (AFM):

As we know that the properties and functioning of thin films is not only affected by its microstructure and chemical or physical composition but also by the interfacial and surface morphology of the films. A rough surfaced substrate tends to have a higher interfacial trapping centers density and also the thin film growth on it will be non-uniform. Hence, polished p-type Silicon <100> wafer has been used in the present research as substrate. Zn_3N_2 and Mg-doped $Zn_3N_2$are semiconductors and can be used in making various semiconductor devices like sensors, detectors etc. Thus, understanding the basic morphology of the thin films is of fundamental importance. AFM is used to examine the surface morphology of the synthesized thin films (TFs) Basic AFM modes estimate the topography of a sample. The only requirement for a sample to be scanned by AFM is that it must be deposited on a flat surface and is hard enough to withstand physical handling during imaging. AFM can provide surface images with sub-optical resolution[22].

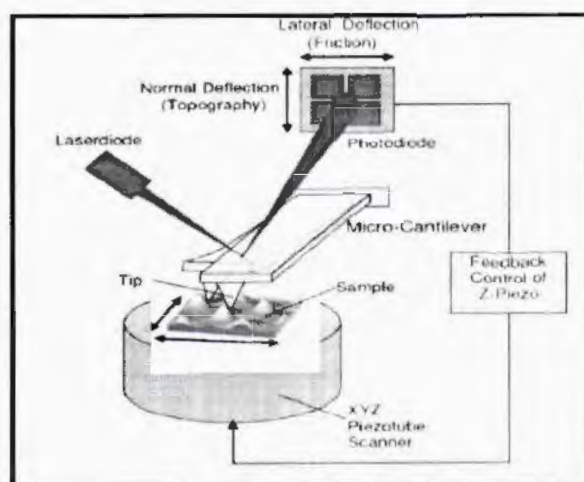

Fig. 3.4: Schematic diagram of AFM.

A typical AFM system shown in Fig 3.4 which consists of a micro-cantilever probe with a sharp tip connected to a piezoelectric actuator with a position sensitive photo detector receiving a laser beam reflected off the end-point of the cantilever beam to provide its deflection feedback [36].Surface morphology can be easily investigated by AFM; an atomic-sized sharp scanning tip is used examine the surface of the sample. Tip is placed at constant height and kept at constant force to get the required force (which is required to break a molecular bond) and height information. This technique is easier than other characterization tools like Scanning Electron Microscopy (SEM), Tunnelling Electron Microscopy (TEM) and optical microscope because no special sample preparation or coating is necessary for imaging.

3.3 Raman Spectroscopy:

Raman spectroscopy is a spectroscopic technique which is used to observe vibrational, rotational and other low-frequency modes in a material. It depends upon inelastic or Raman scattering of monochromatic (single 'λ') light usually from a laser in the visible, near infrared or near ultra-violet range. The interaction of laser light with molecular vibrations, phonons or other excitations in the material results in the shifted energy of the emitted laser photons. This shift in energy occurs due to exchange of energy between the laser photons and material's excitations during an inelastic scattering. Hence, this shifted energy gives the necessary information about the material's vibrational modes.

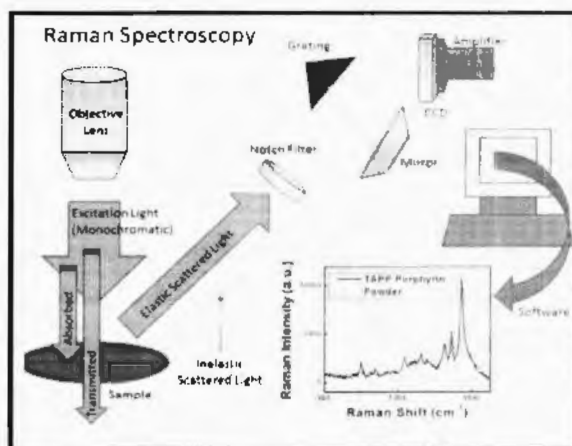

Fig. 3.5: Schematic diagram for Raman Spectroscopy.

The mechanism is very simple. Laser beam is incident on the sample. Electromagnetic radiations from the illuminated part of the sample are collected using a suitable lens and passed through a monochromator. The photons having energy near

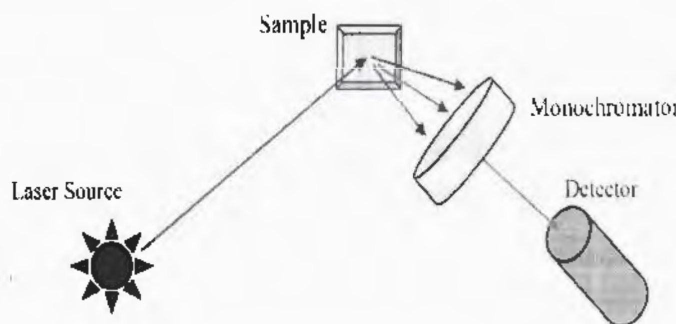

Fig. 3.6: Schematic diagram of Raman spectroscopy.

the incident photons' energy due to elastic (Reyleigh) scattering are filtered out while the rest of the radiation is moved towards the detector.

3.4 Spectroscopic Ellipsometry (SE):

Ellipsometry is an optical characterization technique which is used to accurately figure out the dielectric properties (i.e. complex index of refraction) and thin transparent film's thickness. It uses polarized light and changes in its properties upon reflection and transmission at/through the thin film sample. It is widely used because of its accuracy, non-destructive nature and easy and quick measurement method. Therefore, SE is a standard and suitable measuring technique used in the industry (e.g. microelectronics, solar cells etc) as well as in basic research in all of the

engineering sciences.It is one of the most outstanding and powerful instruments for the characterization of optical properties, especially, of thin-film- and multi-layered materials. In the visible, NIR, and UV, this technique is peculiarly well suited to semiconductors and semiconductor based structures[37].

As we know that, light is an electromagnetic radiation consisting of perpendicularly oscillating electric (**E**) and magnetic (**H**) fields which are perpendicular to the direction of propagation of light as well. For the sake of simplicity, it is represented mathematically only based on electric field **E**. the electric field can be further divided into two components, the supposed polarizations, given as E_p and E_s (E_p gives the amplitude change component and E_s is the component showing change in the phase of the reflected light),these are plane waves mathematically written as

$$E_s = \tilde{E}_s \exp(i\omega t) \quad \text{.................(3.4)}$$

With amplitude $\tilde{E}_s$, ω being the angular frequency and time t and

$$E_p = \tilde{E}_p \exp(i(\omega t - \Delta)) \quad \text{................(3.5)}$$

Where Δ is the phase difference between both polarizations.

3.4.1 Principle of Ellipsometry:

The working principle of ellipsometry is quite simple. A light source is used which radiates un-polarized light. This light is linearly polarized using a polarizer placed at suitable angle. The linearly polarized light will hit the sample at a definite angle ρ. The light will penetrate into the thin film layer and on reaching the thin film and substrate interface, it will get reflected partially.

Fig. 3.7: A Typical Ellipsometer

The emitted light exhibits changes in its properties i.e. the amplitude of both polarizations ($\tilde{E}_s$and $\tilde{E}_p$) as well as the phases Δ between both polarizations will change. The emitted beam will then enter a rotating analyzer, which allows the measure of reflectance for all phases. A photo-detector will then evaluate the intensity of the incoming light beam as a function of the angle of analyzer.

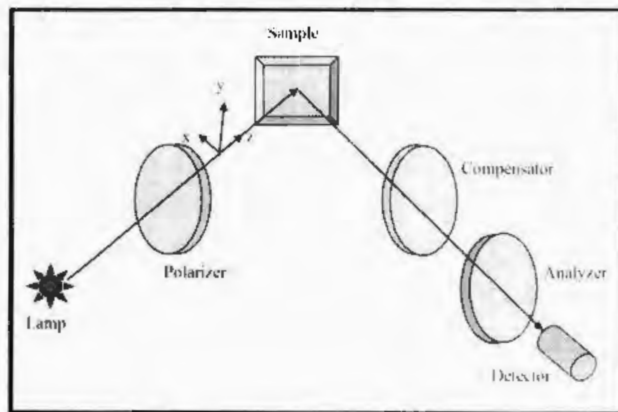

Fig. 3.8: Schematic diagram of basic principle of SE

Measurement results are usually expressed in terms of phase Δ and amplitude ψ related as,

$$\tan \psi \, e^{-i\Delta} = \frac{Rp}{Rs} \quad \text{................(3.6)}$$

Where R_p is the reflectance of p-polarization whereas R_s gives the reflectance of s-polarization.

The calculated data is then transferred to computer for further model-based calculations of film-thickness, refractive indices 'n', extinction coefficients 'k' etc.

Refractive index 'n' gives information about the propagation speed and direction of the wave through the sample. And the extinction coefficient 'k' relates that how much energy of the wave is being absorbed by the material.

3.5 Spectrophotometer:

A spectrophotometer can function in three basic modes; reflection, absorption and transmission. Spectrophotometer is basically used for quantitative study of electromagnetic spectra. Spectrophotometer is an instrument used for measuring the transmission, reflection and absorption of light corresponding to various wavelengths of the light. It measures the fraction of light that reflects or refracts through a given sample. In a spectrophotometer, a light from the lamp is filtered using a monochromator, which chooses light of one peculiar wavelength out of the continuous spectrum. This light passes through the sample. The intensity of the reflected or transmitted light is measured with a photodiode or some other light sensor, and the transmittance, absorption and reflectance for this wavelength is then evaluated.

TH17284

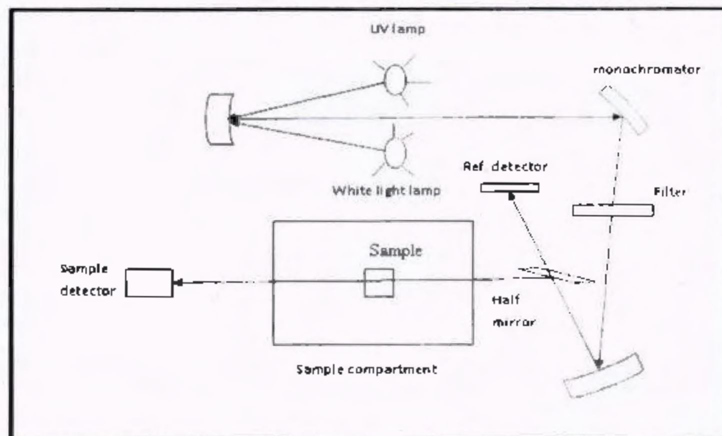

Fig. 3.9: Schematic diagram of a typical spectrophotometer.

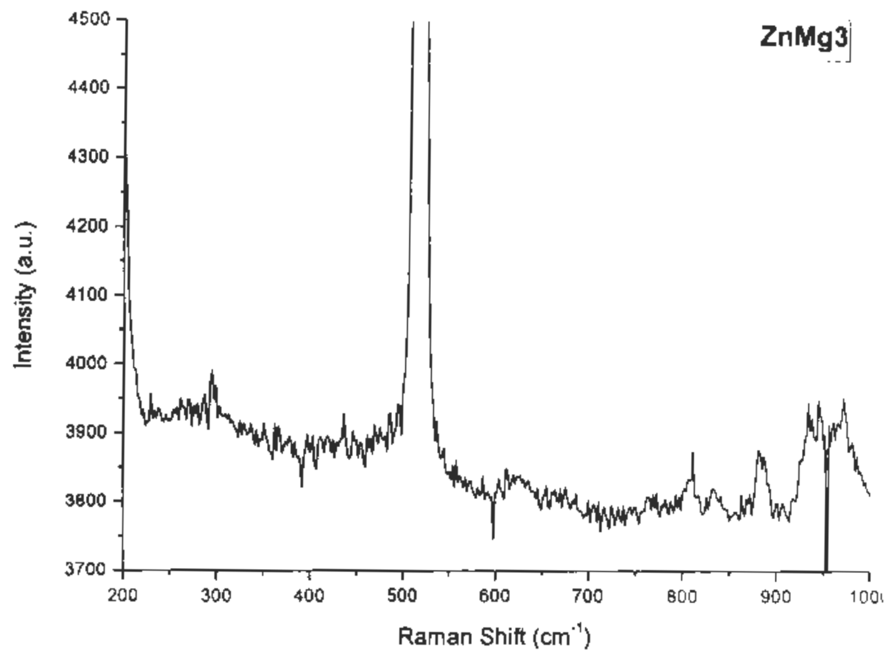

Fig. 4.10: Raman spectra of ZnMg3 (75:25).

Zn-O related Raman vibrational mode appears to have a red shift observed at 517.33cm^{-1}. Fig. 4.10 shows that all the peaks in this thin film are experiencing a red shift which is mainly due to tensile stresses present in the fabricated thin films. These stresses and resulting strains can be removed by annealing.

4.2.5 Zinc Magnesium Nitride thin film (ZnMg4 (65:35)):

The Raman spectra of this thin film also shows an overall red shift. The Zn-N

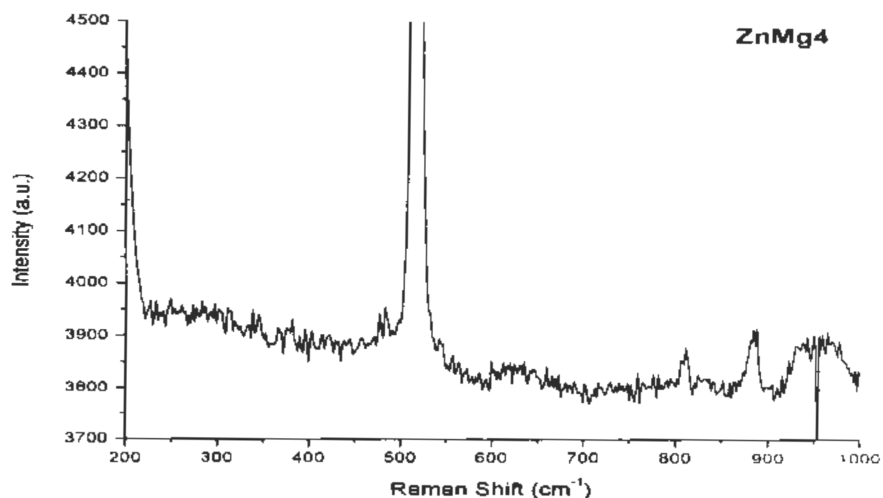

Fig. 4.11: Raman spectra for ZnMg4 (65:35).

related vibrational modes are appearing at 249.29cm^{-1}, 546.10cm^{-1}, 620.37cm^{-1} and 811.09cm^{-1}. Zn-O related Raman mode at 482.66cm^{-1}showed a blue shift whereas vibration modes of Si were showing a red shift being observed at 283.08cm^{-1} and 517.33cm^{-1}[11, 43].

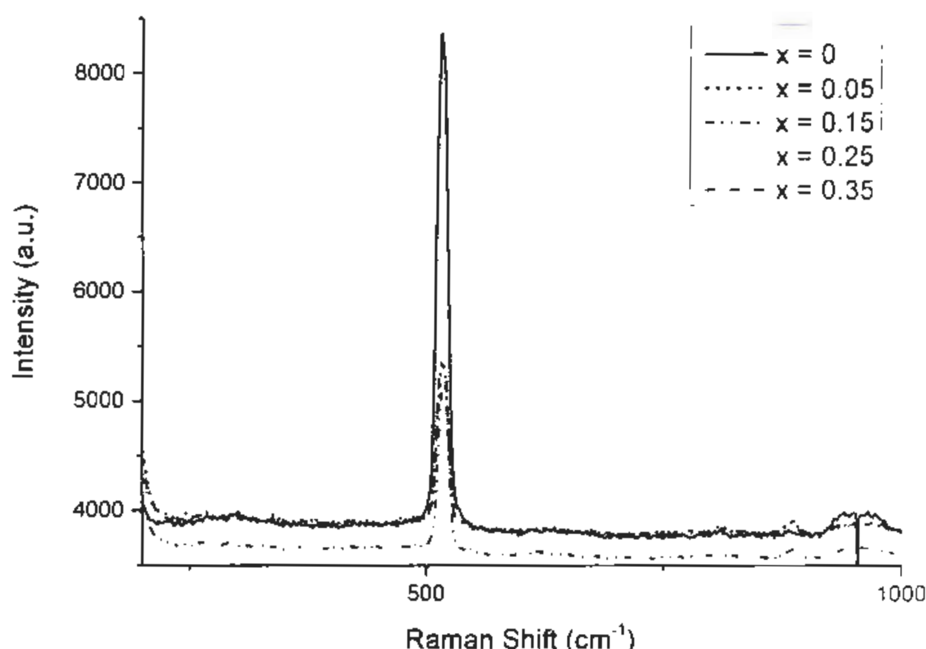

Fig. 4.12: Comparison of $(Zn_{1-x}Mg_x)_3N_2$ with x = 0, 0.05, 0.15, 0.25 & 0.35.

The comparison graph shows an overall decrease in the Raman vibration modes due to an increase in Mg content in the thin films, which clearly explains that the Mg is incorporated in the lattice of zinc nitride structure.

4.3 Electrical Characterization:

The electrical characterizations were carried out using the system mentioned in section3.6. The sheet resistance (R_s) was measured by using a four-point probe setup. Room temperature Hall effect measurements (contact-less) were carried out for calculating the carrier concentration (n), mobility (μ) etc. For measurements, the magnetic field used was of 0.5 Tesla. Hall measurements were repeated 4-5 times for each sample to ensure the reliability of the results. It was observed that the zinc nitride thin films were showing n-type behavior [2, 9, 14, 44]. This n-type behavior is observed to be gradually changing to p-type on increasing the Mg content in thin

Where R_p is the reflectance of p-polarization whereas R_s gives the reflectance of s-polarization.

The calculated data is then transferred to computer for further model-based calculations of film-thickness, refractive indices 'n', extinction coefficients 'k' etc.

Refractive index 'n' gives information about the propagation speed and direction of the wave through the sample. And the extinction coefficient 'k' relates that how much energy of the wave is being absorbed by the material.

3.5 Spectrophotometer:

A spectrophotometer can function in three basic modes; reflection, absorption and transmission. Spectrophotometer is basically used for quantitative study of electromagnetic spectra. Spectrophotometer is an instrument used for measuring the transmission, reflection and absorption of light corresponding to various wavelengths of the light. It measures the fraction of light that reflects or refracts through a given sample. In a spectrophotometer, a light from the lamp is filtered using a monochromator, which chooses light of one peculiar wavelength out of the continuous spectrum. This light passes through the sample. The intensity of the reflected or transmitted light is measured with a photodiode or some other light sensor, and the transmittance, absorption and reflectance for this wavelength is then evaluated.

TH17284

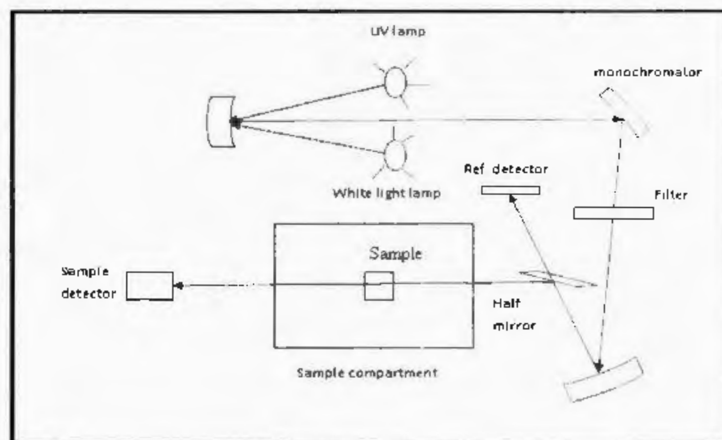

Fig. 3.9: Schematic diagram of a typical spectrophotometer.

3.5.1 UV-VIS Reflectance Spectroscopy:

The same procedure is repeated for wavelengths in a particular range usually UV-Visible range i.e. 200-800nm.UV-Visible spectroscopy is used in Quantitative evaluation of the solutions of transition metal ions and conjugated organic compounds, impurities identification, calculating the band gap (E_g) and analysing the formation of nanoparticles[38].

3.6 Electrical Characterization (IV measurements):

As we know it is the age of miniaturization of electronic components i.e. methods are being acquired for increased efficiency but decreased size of the semiconductor devices. Hence, electrical characterizations are used to evaluate the change in the electrical parameters such as resistivity (ρ), conductivity (σ), carrier concentration (n), electrical mobility (μ) etc. For miniaturization purpose, maximum mobility of charges with minimum carrier concentration (hence area) is preferred for an efficient and smallest possible sized electronic device.

Two-point probing, four-point probing, Hall coefficient calculation, I-V profiling and C-V profiling are some of the most used characterizations to check the electrical properties of the sample under observation.

3.6.1 Sheet Resistance:

The resistance of two-dimensional systems is termed as sheet resistance as in this case for a nominally uniform thickness thin film the depth is minimum. As for resistance the relation is

$$R = \rho \frac{L}{A} \ldots\ldots\ldots\ldots\ldots (3.7)$$

Where 'ρ' is the resistivity of the conductor, 'L' is its length and 'A' is area of cross-section.

If W is taken as the width of the sample and t is its thickness (i.e. area will be, A = Wt), then the resistance of this sample can be written as follows,

$$R = \left(\frac{\rho}{t}\right)\left(\frac{L}{W}\right) = R_S\left(\frac{L}{W}\right) \ldots\ldots\ldots\ldots (3.8)$$

where $R_S = \rho / t$ is the sheet resistance of the sample[39].

As the unit used for the sheet resistance is also Ohm (Ω) (since L/W is unit-less). But to avoid confusion between R and R_s, sheet resistance is determined in unit of "ohms per square (Ω / □)."The '□' shows that it can be any square shaped area may be in mm^2, cm^2, m^2 etc. The L/W ratio can be thought of as the number of unit squares (for any size) of material[39].

Thus, during electrical characterization, a thin film sheet resistance $R_s$is calculated instead of resistance. There are two main methods of calculating value of R_s:

1. Collinear method.
2. Van der Pauw / four-point probing.

In our case, Van der Pauw or four-point probing was carried out for the calculation of sheet resistance R_s. A square area is selected for probing as shown in figure 3.10. Van der Pauw method is a technique which is commonly used to obtain the values of the resistivity (conductivity) and Hall coefficient of any sample. The main and unique advantage of this technique is that it can be efficiently utilized to accurately measure the properties of any arbitrary shaped sample. The only condition for samples is that it must be two-dimensional (thickness much smaller than its length and width). For error reduction, it is preferable that the sample has a symmetric shape with no holes in it.

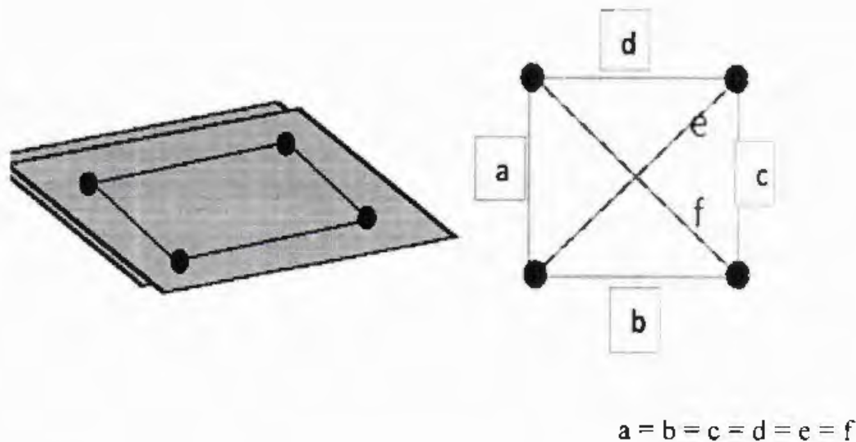

a = b = c = d = e = f

Fig. 3.10: Four – point probing.

To make measurements, a current is circulated in all edges (e.g. I_a) and the corresponding values of voltage (e.g. V_a) are measured respectively. From these values, resistance (R_a) can be calculated using Ohm's law.

In his paper, van der Pauw demostrated that the sheet resistance of the samples can be calculated from the two resistances-one measured along a vertical edge 'R_a' and another being measured along the horizontal one 'R_b'[40]. The actual value of the sheet resistance is related to the above resistances by the van der Pauw formula. The mathematical calculations involved in the above method are as follows:

$$e^{\frac{-\pi Ra}{Rs}} + e^{\frac{-\pi Rb}{Rs}} = 1$$

$$e^{\frac{-\pi}{Rs}}(e^{Ra} + e^{Rb}) = 1$$

$$\ln e^{\frac{-\pi}{Rs}} = \ln \frac{1}{(e^{Ra} + e^{Rb})}$$

$$-\frac{\pi}{Rs} \ln e = \ln \frac{1}{(e^{Ra} + e^{Rb})}$$

$$\Longrightarrow Rs = \frac{-\pi}{\ln {}^{1}/_{(e^{Ra} + e^{Rb})}} \ldots\ldots\ldots\ldots\ldots\ldots (3.9)$$

Or after further simplification, it can also be written as,

$$R_s = \frac{\pi}{\ln(e^{Ra} + e^{Rb})} \ldots\ldots\ldots\ldots\ldots (3.10)$$

Also, carrier concentration (N_s) and mobility (μ) is calculated using this method.

4. Results and Analysis

We prepared our thin film samples using dc sputtering apparatus in thin film fabrication lab, NILOP using different two inches (5.08cm) diameter targets prepared at Material Division, PINSTECH, as discussed earlier in section 2.1, 2.4 and 2.5. These thin films were characterized to observe their structural, optical and electrical properties. Structural analysis was done by X–Ray Diffractometer, D8-Discover HR XRD (Bruker axes, Germany).using Cukα in the range (10°-90°) (λ=0.154nm).. Raman spectra were recorded using μRamboss (Model MST-4000A, South Korea) Raman spectrometer at NILOP, Islamabad. The optical properties were analyzed by using UV-VISIBLE Spectrophotometer for reflectance and spectrometer (Sentec SE-800) Ellipsometry. The electrical properties were observed using four-probe method as already discussed in previous chapter using Van-Der Pauw method. The results obtained after XRD, Raman spectroscopy, spectroscopic reflectance, ellipsometry and electrical characterizations are stated and discussed in the present chapter.

4.1 Structural Analysis (XRD):

The XRD measurements of all the thin films samples were carried out using X-ray Diffractometer in the range 10°-90° (λ = 0.154nm). The discussion and analysis of XRD patterns is given separately for each sample. The software used for this purpose in X'pert HighScore.

4.1.1 Zinc Nitride Pure Zn_3N_2:

To evaluate the structure, lattice constants and other such parameters of all the prepared thin films, XRD analysis was performed. Fig. 3.1 shows the wide angle x-ray diffraction pattern of pure zinc nitride thin films named as ZnMg0 with 0% Mg content in the target. Diffraction peaks of zinc nitride appeared at 2θ = 34.12°, 36.84° and 53.78° corresponding to reflections from (321), (400) and (440) planes respectively (JCPDS Card No. 35-0762)[14]. As it is evident from literature that on removing the deposited zinc nitride thin films from vacuum chambers, they get oxidized to some extent[5, 12, 14].Hence, at 2θ = 36.44° and 62.26°, small reflection peaks corresponding to (101) and (103) planes of zinc oxide were observed(JCPDS Card No. 01-1150 & 36-1451) [29].

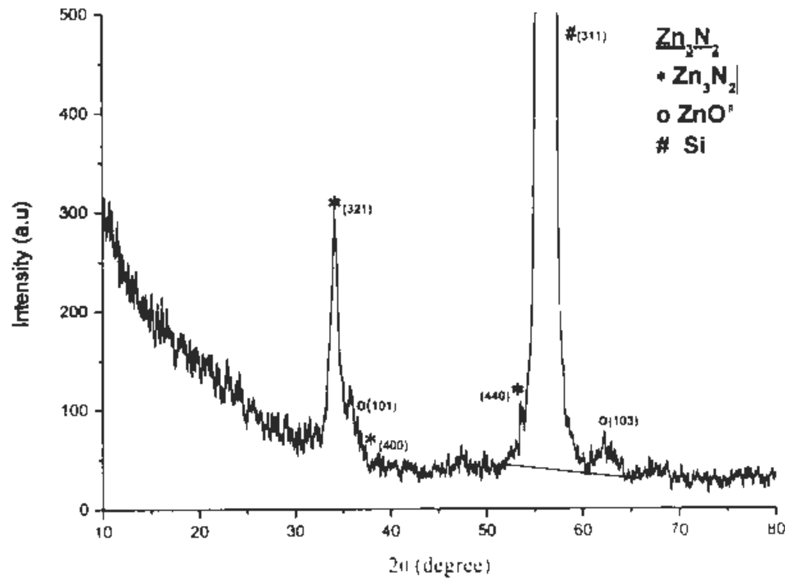

Fig. 4.1: X-ray diffraction pattern of Zn_3N_2.

The XRD pattern of pure zinc nitride thin film deposited on p-type Silicon substrate shows an overall shifting of peaks towards lower 2θ values than the standard ones. The main and very intense peak at about 2θ = 56.14° is due to the silicon substrate. The calculation of lattice constants using the Bragg's law and lattice constant formula in terms of miller indices is as follows:

$$2d \sin\theta = n\lambda \qquad (4.1)$$

$$\Rightarrow d = \frac{\lambda}{2\sin\theta} \qquad (4.2)$$

Using above relation in the formula of lattice constant 'a', we get,

$$a = \frac{\lambda}{2\sin\theta}\sqrt{(h^2 + k^2 + l^2)} \qquad (4.3)$$

The table below shows the grain size (using eq. 3.3) and micro-strain calculations for the most prominent peaks of the first sample.

2θ (deg.)	θ (deg.)	FWHM 'β'		Grain size 'D'(nm)	Micro-strains 'ε'($x10^{-3}$)
		in deg.	in rad. ($x10^{-3}$)		
56.14	28.07	1.24	0.0216	7.27	10.1
34.12	17.06	0.58	0.0101	14.35	8.23

Table 4.1: Structural parameters of Zn_3N_2.

The positive values of micro-strains are calculated by the formula used for thin films in literature[29, 41] i.e.

$$\text{Micro-strains} = \frac{\beta}{4\tan\theta} \quad \ldots\ldots\ldots\ldots\ldots(4.4)$$

Calculated value of lattice constant 'a' (nm)	Theoretical value of lattice constant 'a' (nm)	Difference (nm)
0.9733	0.97769	4.39×10^{-3}

Table 4.2: Comparison of obtained and theoretical values of 'a'.

Grain size is calculated by using Debye-Schrrer's formula (eq. 3.3). The value of lattice constant 'a' was calculated by using eq. 4.3. As we know the thin films fabricated are un-annealed yet so it is clear from the positive values of the micro-strains calculated in table 4.1 as well as the value of the lattice constant 'a' can easily be seen increasing with an increase in the Mg content in samples discussed ahead and the stresses in action are tensile stresses hence resulting in an increase in the volume of the unit cell. Here, the value of 'a' is decreased as compared to the theoretical value which shows a decrease in unit cell's volume. These can be reduced or relaxed by annealing the samples at suitable temperatures.

4.1.2 $(Zn_{1-x}Mg_x)_3N_2$ (x = 0.05))

The value of x that is the concentration of the magnesium (Mg) is changed in the targets by some fixed ratios. In our second sample, x = 5% = 0.05. The XRD

graph of the second sample shows reflections at 2θ = 33.94°, 36.16° and 79.86° of Zn_3N_2 structure for planes (321), (400) and (651) respectively. The reflection at 2θ = 56.84° corresponds to reflection from (311) plane of Silicon. At 2θ = 57.34°, reflection is present due to Magnesium (Mg) plane (110). This means that there is some Mg left in metallic form which did not react with Zn or N_2. At 2θ = 30.44°, the reflection occurs due to ZnO plane (100). The starting raised part and peaks of the graph are system generated. The structural parameters calculated as in the case of first sample are stated in table 4.3.

2θ (deg.)	θ (deg.)	FWHM 'β'		Grain size 'D'(nm)	Micro-strains 'ε'(x10⁻³)
		in deg.	in rad. (x10⁻³)		
30.44	15.22	0.25	4.36	32.95	4.01
79.86	39.93	0.4	6.98	26.08	2.06
56.84	28.42	0.16	2.79	55.48	1.29

Table 4.3: Structural parameters of ZnMg1 (95:05).

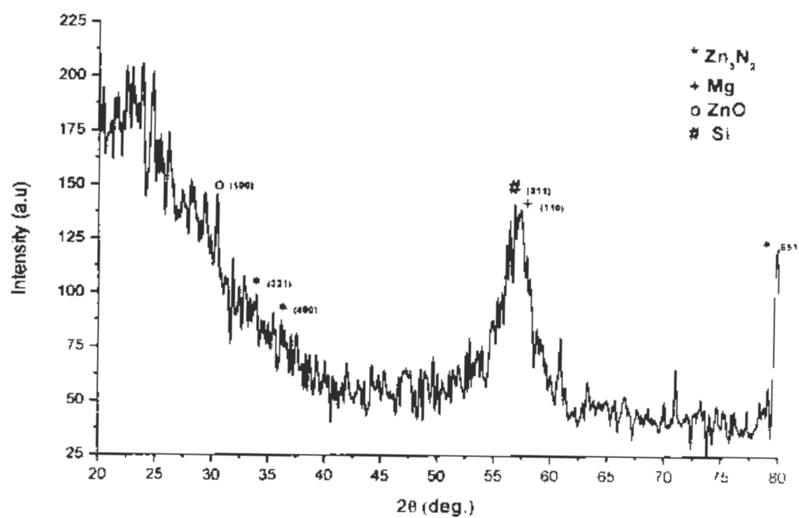

Fig. 4.2: X-ray diffraction pattern of ZnMg1 (95:05).

The mean value of lattice constant 'a' was calculated to be 0.9747nm. It cannot be compared to any theoretical value from the literature as no one has yet fabricated zinc nitride thin films with any other doping in it. It is clear that the value of 'a' is increasing as we increase the Mg content in Zn_3N_2 thin films,a = 0.9747nm. Also, the micro-strains are positive which indicates the presence of tensile stresses which will relax on annealing the thin films[42].

4.1.3 $(Zn_{1-x}Mg_x)_3N_2$ (x = 0.15):

The XRD pattern of ZnMg2 with x = 15% or 0.15 clearly shows the reflections at 2θ = 35.44°, 44.2°, 52.86°, 71.04° and 79.86° for the planes (400), (332), (440), (721) and (651) respectively. The graph clearly shows the peaks for Mg at 57.34° and 60.9°for planes (110) and (103) respectively. At 2θ = 56.86°, Si peak appeared. A small peak indicating the presence of ZnO was observed at 30.44° corresponding to x-rays' reflection from (100) plane.

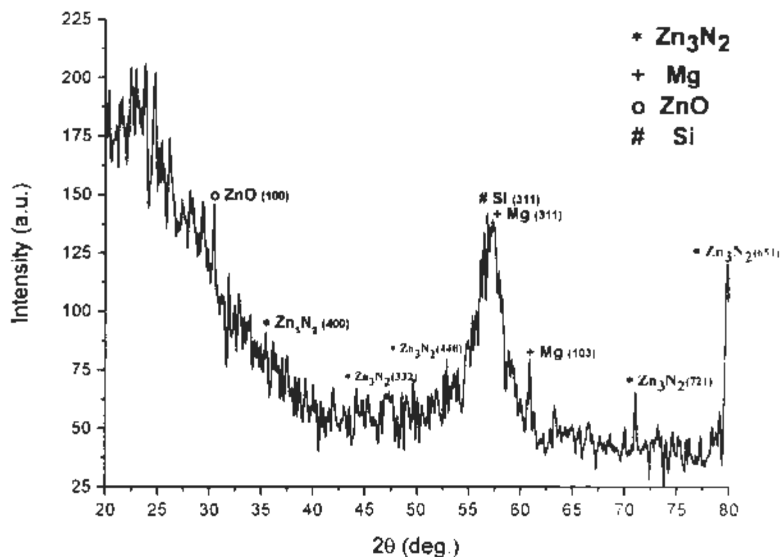

Fig. 4.3: X-ray diffraction pattern of ZnMg2 (85:15).

The starting raised part and peaks of the graph are system generated. The structural parameters calculated as in the case of first sample are stated in table 4.4.

2θ (deg.)	θ (deg.)	FWHM 'β'		Grain size 'D'(nm)	Micro-strains 'ε'($x10^{-3}$)
		In deg.	in rad. ($x10^{-3}$)		
30.44	15.22	0.23	4.01	35.82	3.68
56.86	28.43	0.12	2.09	75.41	0.965
71.04	35.52	0.24	4.19	40.64	1.47
79.86	39.93	0.35	6.11	29.58	1.82

Table 4.4: Structural parameters of ZnMg2 (85:15).

The positive strains shows that the tensile stresses are again in action and also the value of 'a' is continuously increasing. In present sample, a = 0.9801nm, that means volume of unit cell is increasing also due to more and more incorporation of the Mg in the crystal lattice. There is a decrease in overall crystallinity of the thin film which can be improved by thermal processing like annealing etc.

4.1.4 $(Zn_{1-x}Mg_x)_3N_2$ (x = 0.25):

The XRD pattern of sample with x = 25% or 0.25 ratio of Mg in the target with 0.75 Zn shows that due to some unknown reason formation of Zn_3N_2 was not as much as in other samples hence, a few lower intensity peaks for Zn_3N_2were observed. Whereas, it is evident from the graph that pure Mg is deposited as it is on the substrate and a small peak indicating the presence of $Mg_3N_2$was also observed at 50.82° corresponding to plane (440). At 2θ = 34.3°, 34.52° and 43.24°, peaks of $Zn_3N_2$for planes (321), (400) and (332) are visible but with relatively lower intensity. Another peak for Zn_3N_2at 2θ = 70.42° is also appearing for (721). The values of 2θ along with the planes and materials related to the peaks is given in the figure no. 4.4.

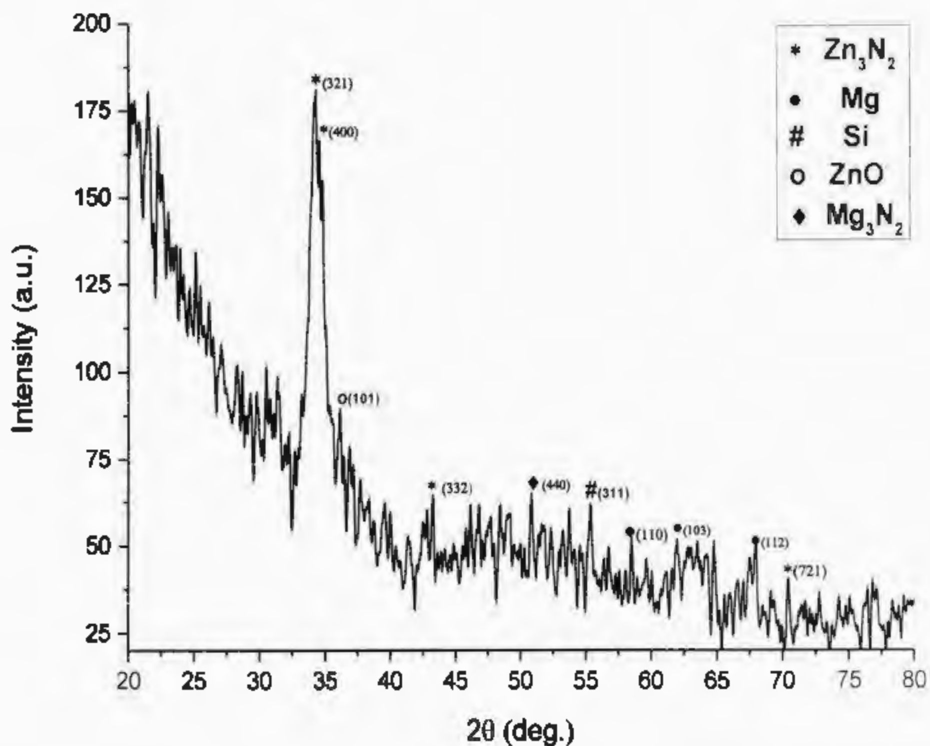

Fig. 4.4: X-ray diffraction pattern of ZnMg3 (75:25).

2θ (deg.)	Material	(hkl)
34.16	Zn_3N_2	(321)
34.52		(400)
43.24		(332)
70.42		(721)
58.5	Mg	(110)
61.96		(103)
67.98		(112)
55.36	Si	(311)
50.82	Mg_3N_2	(440)

Table 4.5: ZnMg3 (75:25) 2θ values along with corresponding planes (hkl).

Due to some unknown ambient condition Mg was not able to react properly to form zinc magnesium nitride, instead magnesium nitride and pure magnesium were deposited. The graph also shows that the crystallinity of the films is deteriorating which can be enhanced upon further thermal processing of the thin films. This could be understand with the fact that the deposited film contains the different grains with different chemical composition.

2θ (deg.)	**θ (deg.)**	**FWHM 'β'**		**Grain size 'D'(nm)**	**Micro-strains 'ε'(x10^{-3})**
		In deg.	**in rad. (x10^{-3})**		
34.18	17.15	0.04	0.698	207.82	0.565
34.52	17.26	0.1	1.74	83.41	1.40
43.24	21.62	0.08	1.395	106.87	0.8799
55.36	27.68	0.13	2.27	68.94	1.08

Table 4.6: Structural parameters of ZnMg3 (75:25).

Positive micro-strains and increased value of a (average) = 0.9943nm (and d-spacing) indicates tensile stresses and increased volume of the unit cell implies the incorporation of Mg as well as magnesium nitride. This increase could be attributed to the incorporation of Mg nanocrystals at the interstitial sites or due to the bonding between Mg and nitrogen atoms as evident through Mg_3N_2 peak. The peaks are mostly shifted towards the lower values of 2θ due to tensile strains.

4.1.5 $(Zn_{1-x}Mg_x)_3N_2$ (x = 0.35):

This thin film's target had 35% Mg and 65% Zn in it. The XRD pattern shows different reflections related to different materials which is given in the form of a table along with their planes (hkl).

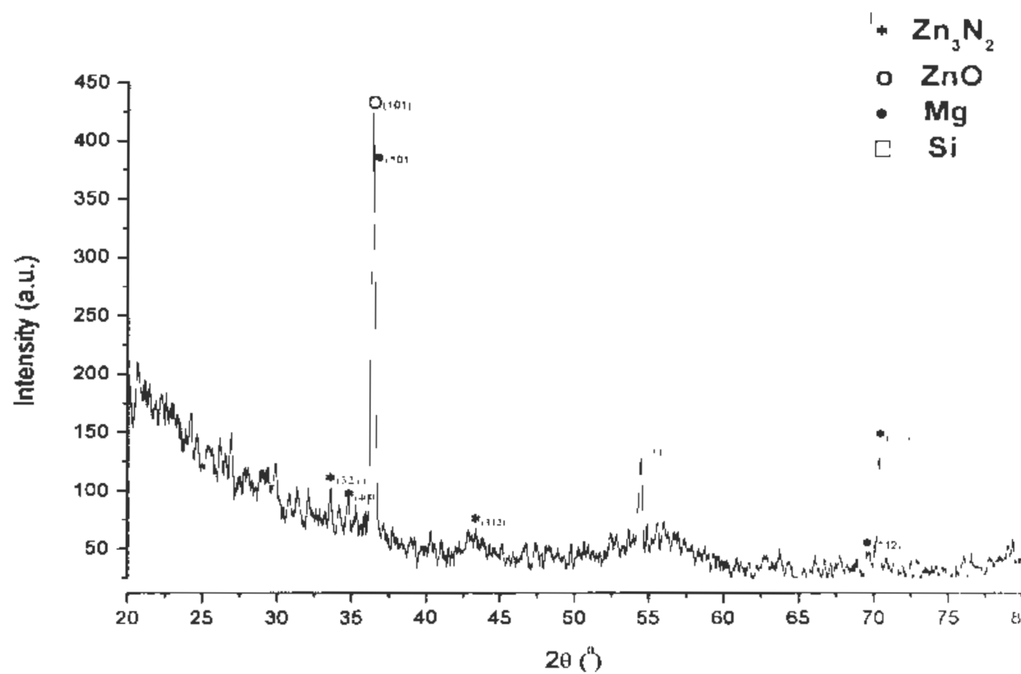

Fig. 4.5: X-ray diffraction pattern of ZnMg4 (65:35).

2θ (deg.)	Material	(hkl)
33.58	Zn_3N_2	(321)
34.84		(400)
43.34		(332)
70.32		(721)
36.44	Mg	(101)
56.92		(110)
69.52		(112)
55.46	Si	(311)
36.38	ZnO	(101)

Table 4.7: ZnMg4 (65:35) 2θ values along with corresponding planes (hkl).

The graph implies maximum oxidation of ZnMg4 in ambient condition and improved crystallinity as well. The average value of a = 0.9967nm for this thin film

sample again tensile stresses are playing their role in increased d_{hkl} and unit cell volume as well.

2θ (deg.)	θ (deg.)	FWHM 'β'		Grain size 'D'(nm)	Micro-strains 'ε'(x10⁻³)
		in deg.	in rad. (x10⁻³)		
36.38	18.19	0.26	4.54	32.14	3.45
70.32	35.16	0.22	3.84	44.15	1.36
54.48	27.24	0.25	4.36	35.75	2.12

Table 4.8: Structural parameters of ZnMg4 (65:35).

The comparison graph of XRD for all the samples is shown below for a quick overview. It is clear how the peaks are shifting and rising with the increase in Mg content. However, ZnMg3 curve is quite similar to ZnMg0 curve. It is evident from the XRD data that the sample with 25% Mg has almost the similar pattern as pure Zn_3N_2 with increased lattice constant. So x = 0.25 is probably the optimized value of doping percentage.

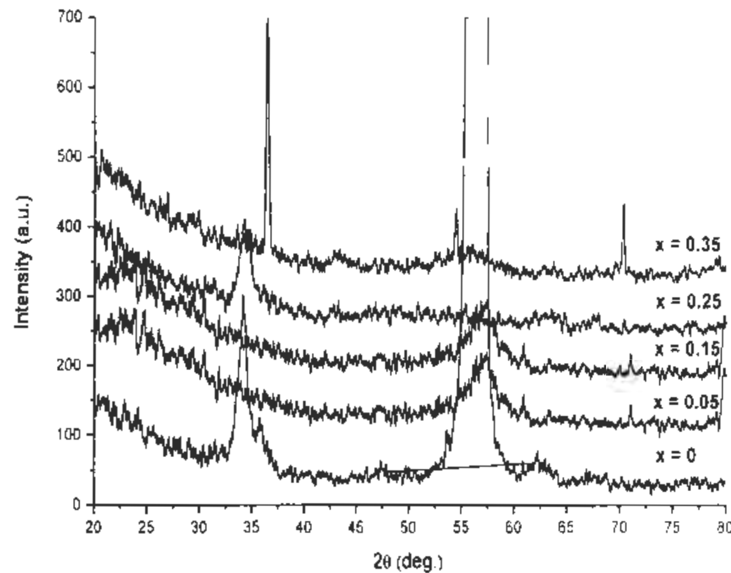

Fig. 4.6: XRD patterns' comparison of $(Zn_{1-x}Mg_x)_3N_2$ with x = 0, 0.05, 0.15, 0.25 & 0.35.

4.2 Raman Spectroscopy:

The Raman spectroscopy of the fabricated thin films was done to check the characteristic vibrational and rotational modes of zinc nitride and the effect of Mg content on the vibrational modes of the synthesized thin films. All the samples have shown an overall red shift in the characteristic peak of Si (100) i.e. 302cm^{-1} and 520cm^{-1}[11, 15, 43].

4.2.1 Zinc Nitride thin films (Zn_3N_2):

A Raman spectra for pure zinc nitride thin films fabricated by using a pure Zn target in N_2atmosphere was recorded using the system mentioned in section 3.3. Fig. 4.7 shows the Raman spectra of zinc nitride thin films. The pattern exhibits two characteristic Raman peaks for Zn-N related vibrations at about 267.19cm^{-1}[15] and 811.09cm^{-1}[11]. Also Zn-N related vibrational mode is observed at 627cm^{-1} with a blue shift[11].The characteristic Raman-active vibration modes are observed to have a small shift (blue or red) due to the un-annealed nature of the thin films or it can be said due to the presence of the tensile stresses as discussed in XRD analysis. This shift might be reduced upon annealing. The main intense peak at 515.41cm^{-1}represents the first-order Si Raman mode[11, 43]. It can also be observed that this peak is shifted towards lower wave number hence showing a red shift. At 300.9cm^{-1}, another Si Raman peak is observed with a red shift[43].

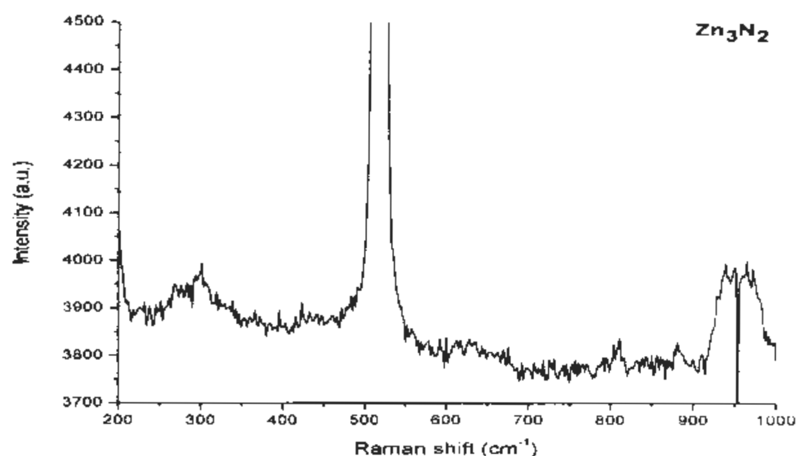

Fig. 4.7: Raman spectra of Zinc nitride thin films Zn_3N_2.

At 422.57cm^{-1}, there is a Raman peak of Zn-O related vibrational mode proving the presence of oxides as well as nitrides in the thin film also a wide peak just below

1000cm^{-1} exhibits 2nd order Si Raman mode[43]. It shows a blue shift in the Raman peak i.e. shift towards higher Raman number. As here blue shift is prominent which means there is a decrease in the bond length. Hence these results are comparable to those of XRD which gives a reduced value of lattice constant 'a' depicting an overall decrease in the unit cell's volume.

4.2.2 Zinc Magnesium Nitride thin film (ZnMg1 (95:05)):

The Raman spectrum of zinc nitride thin film with 5% Mg content in the target used for sputtering is shown in the fig. 4.8. Fig. 4.8 shows the Zn-N related vibrations at 620.37cm^{-1} (originally at 620cm^{-1}) and 809.25cm^{-1} (originally at 825cm^{-1}) showing an overall red shift[11]. The Raman peaks at 267.19cm^{-1}(originally at 257cm^{-1}) with a blue shift shows the characteristic Raman-active vibrations mode[15].

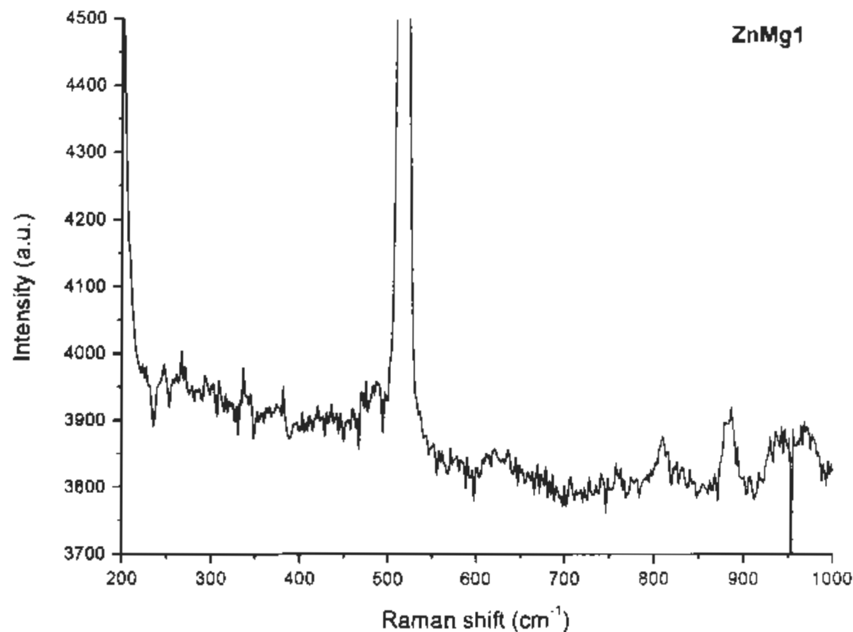

Fig. 4.8: Raman spectra for ZnMg1 (95:05).

Another Raman peak at 436.18cm^{-1}(originally at 437cm^{-1}) shows the presence of Zn-O related vibration[43] with a red shift. 2nd order Si wide Raman peak is appearing below 1000cm^{-1} with a red shift.

4.2.3 Zinc Magnesium Nitride thin film (ZnMg2 (85:15)):

Zn-N related vibrations in thin films ZnMg2 were observed with Raman peaks at 257.25cm^{-1}(characteristic Raman-active vibration mode), 882.69cm^{-1}(Zn-N related

vibrations in Zinc nitride and oxy-nitride films[11]), 557.58cm^{-1}(characteristic Raman-active vibration modes) and 614.49cm^{-1}(Zn-N related vibrations).The first two are showing a blue shift (towards higher Raman number) and the last two are showing a red shift (towards lower Raman number)[11, 15]. Zn-O related vibrational mode is observed at 486.52cm^{-1} with a blue shift.

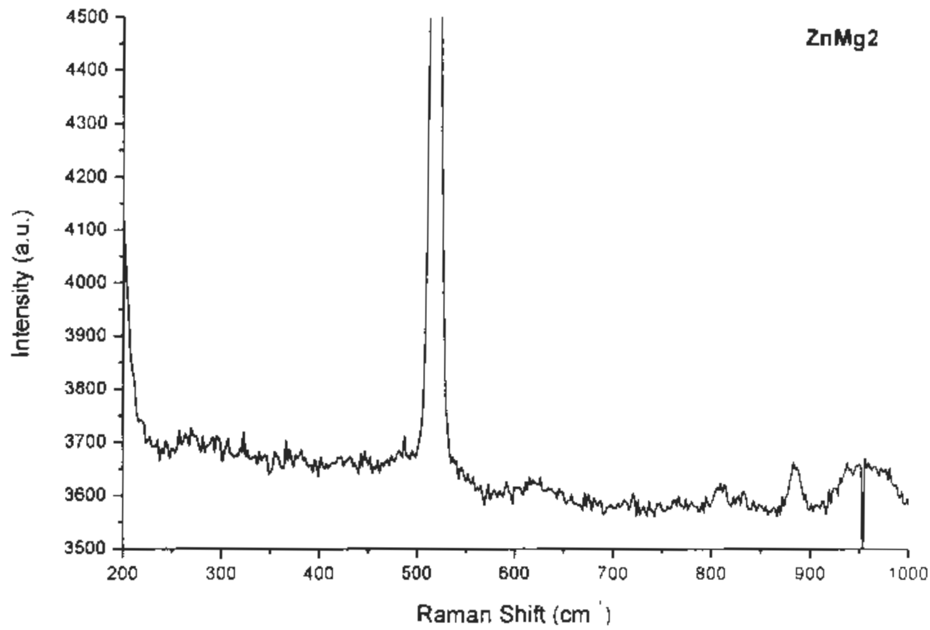

Fig. 4.9: Raman spectra for thin film ZnMg2 (85:15).

Raman peaks for Si are appearing at 336.4cm^{-1} and 515.41cm^{-1} with a blue and red shift respectively[43].

4.2.4 Zinc Magnesium Nitride thin film (ZnMg3 (75:25)):

An overall red shift was observed in the vibration modes of Si (294.96cm^{-1},517.33cm^{-1}) and those of Zn-N related and characteristic vibration modes were observed at 229.34cm^{-1}, 557.58cm^{-1} and 831.36cm^{-1}.

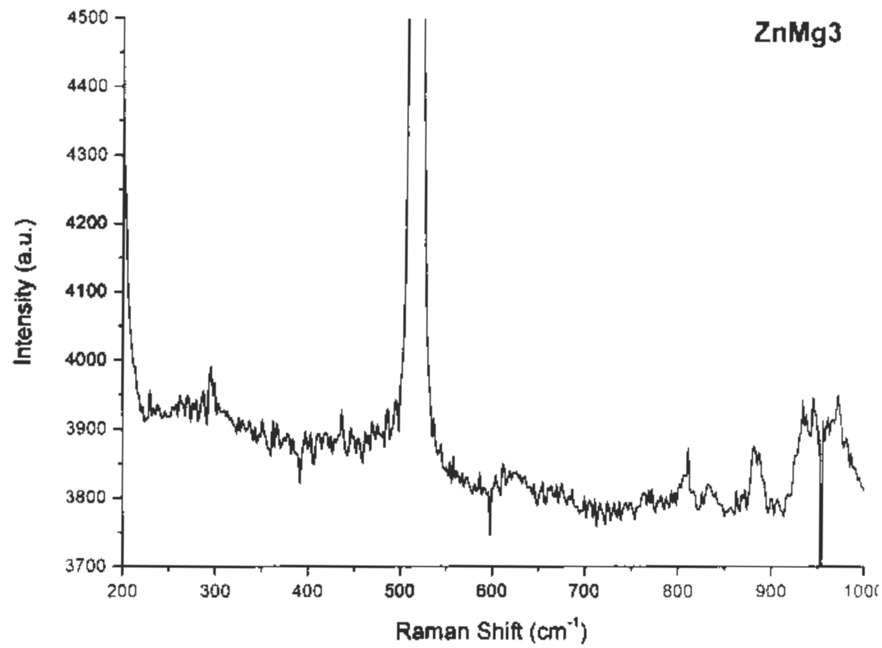

Fig. 4.10: Raman spectra of ZnMg3 (75:25).

Zn-O related Raman vibrational mode appears to have a red shift observed at 517.33cm^{-1}. Fig. 4.10 shows that all the peaks in this thin film are experiencing a red shift which is mainly due to tensile stresses present in the fabricated thin films. These stresses and resulting strains can be removed by annealing.

4.2.5 Zinc Magnesium Nitride thin film (ZnMg4 (65:35)):

The Raman spectra of this thin film also shows an overall red shift. The Zn-N

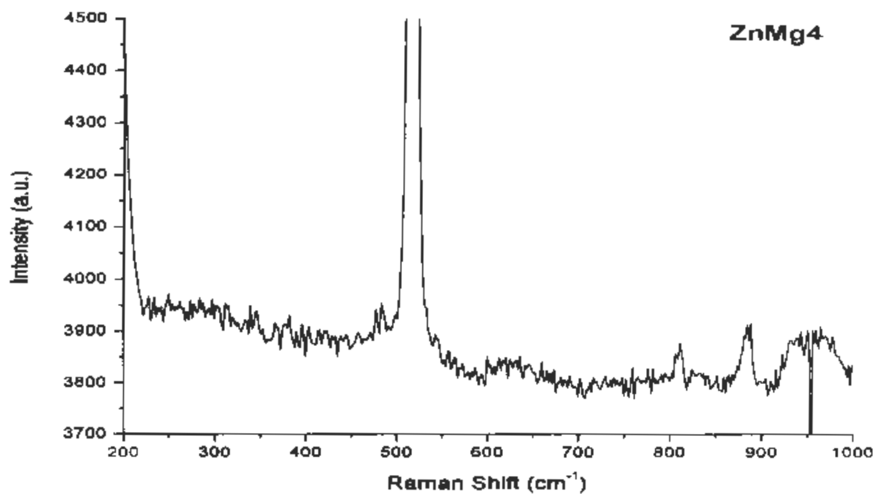

Fig. 4.11: Raman spectra for ZnMg4 (65:35).

related vibrational modes are appearing at 249.29cm^{-1}, 546.10cm^{-1}, 620.37cm^{-1} and 811.09cm^{-1}. Zn-O related Raman mode at 482.66cm^{-1}showed a blue shift whereas vibration modes of Si were showing a red shift being observed at 283.08cm^{-1} and 517.33cm^{-1}[11, 43].

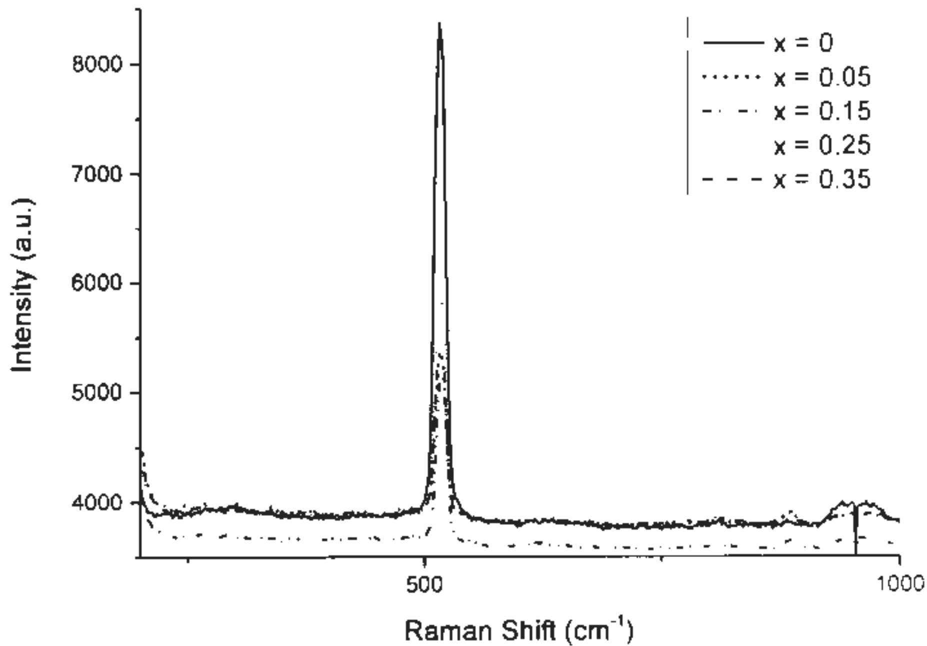

Fig. 4.12: Comparison of $(Zn_{1-x}Mg_x)_3N_2$ with x = 0, 0.05, 0.15, 0.25 & 0.35.

The comparison graph shows an overall decrease in the Raman vibration modes due to an increase in Mg content in the thin films, which clearly explains that the Mg is incorporated in the lattice of zinc nitride structure.

4.3 Electrical Characterization:

The electrical characterizations were carried out using the system mentioned in section3.6. The sheet resistance (R_s) was measured by using a four-point probe setup. Room temperature Hall effect measurements (contact-less) were carried out for calculating the carrier concentration (n), mobility (μ) etc. For measurements, the magnetic field used was of 0.5 Tesla. Hall measurements were repeated 4-5 times for each sample to ensure the reliability of the results. It was observed that the zinc nitride thin films were showing n-type behavior [2, 9, 14, 44]. This n-type behavior is observed to be gradually changing to p-type on increasing the Mg content in thin

films as can easily be seen by the values of surface carrier density. The volume carrier density is positive which may be due to the dominating contribution of p-type Si substrate of the thin films.

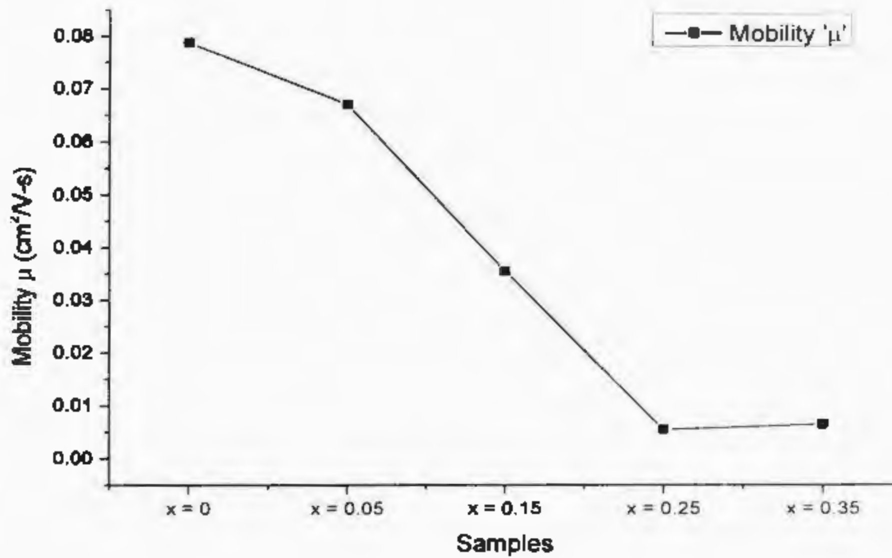

Fig. 4.13: Graph of mobility (μ) of $(Zn_{1-x}Mg_x)_3N_2$ with x = 0, 0.05, 0.15, 0.25 & 0.35.

Samples	Sheet resistance 'R_s' (Ω/□)	Surface carrier density 'n_s'	Volume carrier density 'n'(cm^{-3})	Mobility 'μ' (cm^2/Vs)	Conductivity 'σ' (mho/cm^2)
ZnMg0	2.051×10^5	-4.20137×10^{14}	2.64×10^{20}	0.07874	0.657
ZnMg1	1.04904×10^6	-1.04499×10^{14}	4.85×10^{19}	0.0671	0.117
ZnMg2	5.471×10^5	-1.03534×10^{15}	1.19395×10^{20}	0.03555	0.372
ZnMg3	6.599×10^5	-4.68893×10^{15}	2.74×10^{20}	0.00547	0.301
ZnMg4	1.05093×10^6	-1.69459×10^{15}	1.11×10^{21}	0.00643	0.189

Table 4.9: Electrical values calculated by 4-point probing.

Fig. 4.14 and 4.13 show the graphical representation of the volume carrier concentration (n) and mobility (μ) for the samples whereas Fig. 4.15 shows the calculated values of sheet resistance (R_s) plotted for each of the samples.

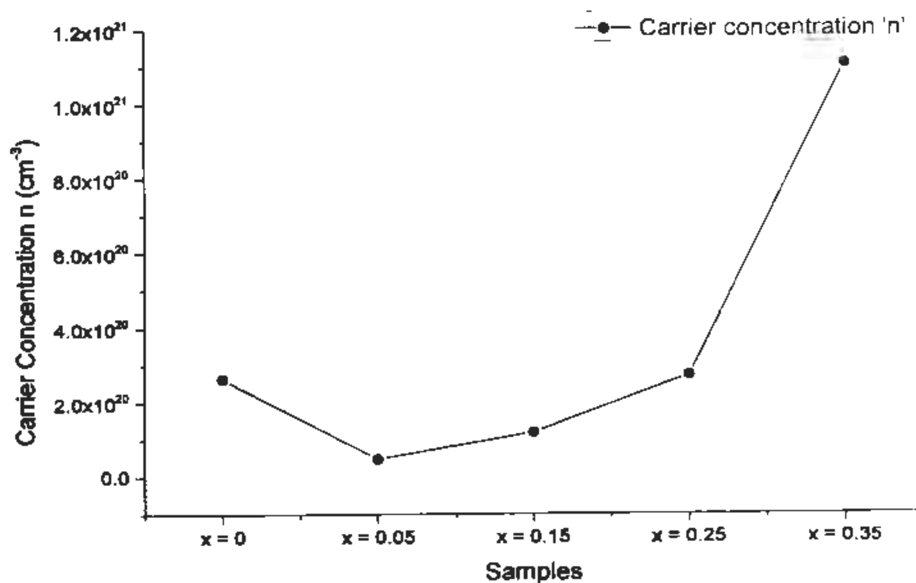

Fig. 4.14: Graph of carrier concentration (n) of $(Zn_{1-x}Mg_x)_3N_2$ with x = 0, 0.05, 0.15, 0.25 & 0.35.

Above graphs clearly show that mobility value was overall decreasing at first, became minimum for ZnMg3 (75:25) but drastically increased for ZnMg4 (65:35). The

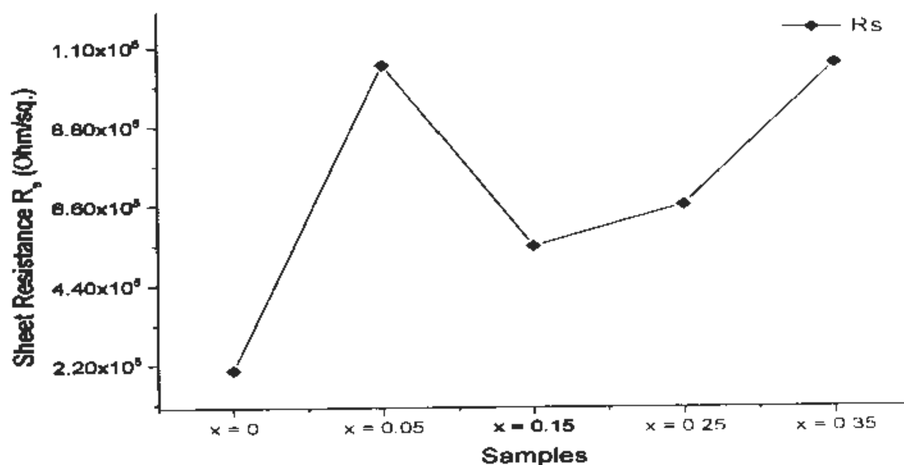

Fig. 4.15: Graph of sheet resistance (R_s) of $(Zn_{1-x}Mg_x)_3N_2$ with x = 0, 0.05, 0.15, 0.25 & 0.35.

decrease in mobility may be due to the presence of impurity scattering mechanism and decrease in crystallinity [14]. But the mobility is decreasing and almost remains same for samples with x = 0.25 & 0.35. In the starting samples, the decreasing mobility and carrier concentration indicates a decrease in the crystallinity of the thin films. For ZnMg4 (x = 0.35), the increasing carrier concentration with decreased mobility indicates the dominance of impurity scattering in this sample. It is clear from a previous work that ZnMg4 (65:35) sample gives a better result due to this specific ratio[24]. Also, the value of sheet resistance is minimum for ZnMg0 (Zn_3N_2) and around maximum for ZnMg1 and ZnMg4 as clearly shown by fig. 4.15. More appropriate results will be revealed upon annealing of thin films. The oxidation of zinc atoms may be the reason of provision of one extra electron hence increasing the volume carrier density. The conductivity of the samples lies in the range of semi-conductors.

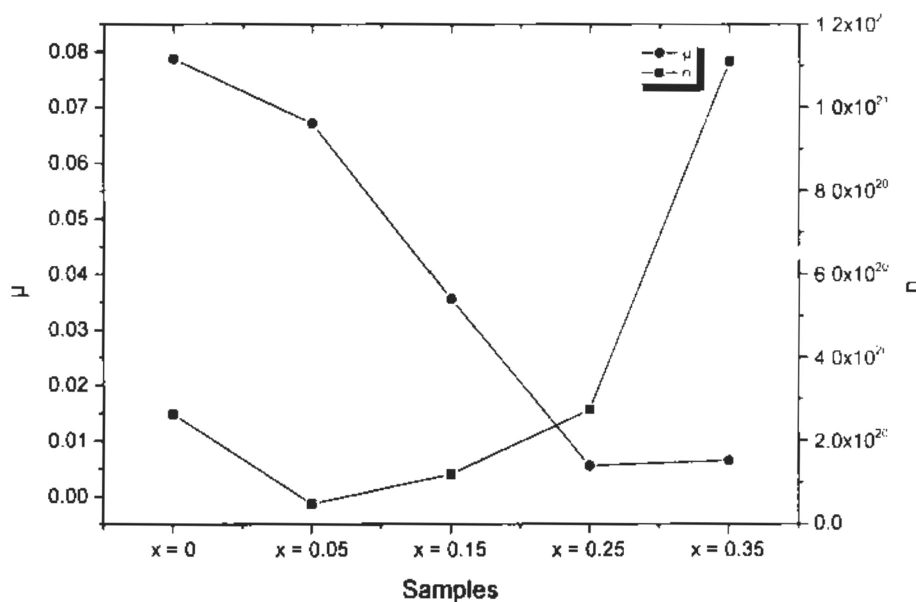

Fig. 4.16: Comparison graph of mobility and carrier density of $(Zn_{1-x}Mg_x)_3N_2$ with x = 0, 0.05, 0.15, 0.25 & 0.35.

Fig 4.16 shows that the mobility 'μ' of the samples is decreasing with increasing charge carrier density which indicates that the impurity scattering

mechanism is

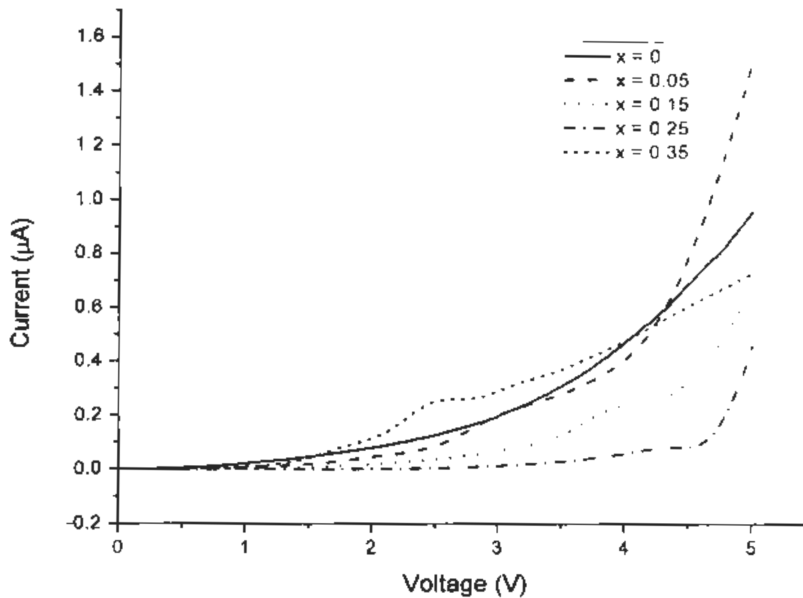

Fig. 4.17: IV curves of $(Zn_{1-x}Mg_x)_3N_2$ with x = 0, 0.05, 0.15, 0.25 & 0.35.

becoming more and more dominant and if it was a reciprocated situation (i.e. μ increasing but n decreasing), the grain boundary scattering would be dominating[14].

The IV-curves (Fig. 4.17) of the samples shows the semi-conducting behaviour of the samples. As the carrier density was found to be maximum for ZnMg1 (x = 0.05), its IV curve is higher than all others.

4.4 Optical Characterizations:

Two optical characterizations techniques were used to investigate the optical properties of all the samples. One of the techniques used is UV-VIS reflectance and other is Spectroscopic Ellipsometry (SE). Both of these techniques are discussed in the previous section along with their basic mechanisms. The optical properties of so fabricated thin films given by above two techniques are found to be in accordance with each other.

4.4.1 UV-VIS Reflectance Spectroscopy:

There are basically three types of this spectroscopy; transmission, reflectance and absorption. The value and type of the band gap of Zn_3N_2 thin films was estimated by using the UV-VIS reflectance data. Transmittance mode was not used as our substrate

i.e. p-Si is not transparent hence not supporting the transmittance of incident light. There are some contradictions in the type and value of the optical band gap of zinc nitride thin films in comparison to the previously reported data. Mostly band gap is reported to be direct one. There is a wide difference between the obtained values from two groups of researchers: 1.01-1.47eV and 3.2eV[9].

The reflectance spectra of pure zinc nitride thin film is given in fig. 4.18. The analysis of the data to obtain the value of E_g was done by using the Kubelka-Munk function as used earlier[1]. This function gives the ratio of absorption coefficient and scattering coefficient as follows,

$$F(R) = \frac{\alpha}{S} = \frac{(1-R)^2}{2R} \quad \ldots\ldots\ldots\ldots\ldots\ldots\ldots (4.4)$$

Where α = absorption coefficient, S = scattering coefficient, R = reflectance.

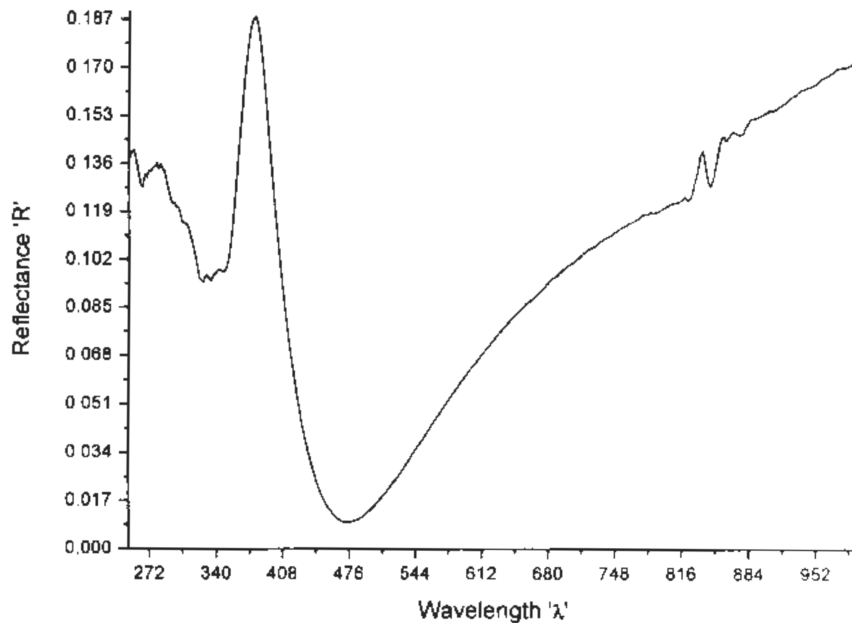

Fig. 4.18: Reflectance curve for $(Zn_{1-x}Mg_x)_3N_2$ (x = 0).

As S is assumed to be constant which is usually justifiable around band edge. Hence, F(R) is proportional simply to α.

As for calculations of $E_g$value of semiconductors, Tauc and Menth method is used in analysis[45].

$$(h\nu\alpha)^m = A(h\nu - E_g) \ldots\ldots\ldots\ldots\ldots (4.5)$$

where h, v, α, E_g, m and A are Plank's constant, frequency of the incident light, absorption coefficient and constants respectively.

For direct band gap m = 2 is used and for indirect band gap semiconductor, its value is $\frac{1}{2}$. Here, we assumed that Zn_3N_2 has a direct band gap as reported by many groups, the square of (hv F(R)) is proportional to (hv - E_g).

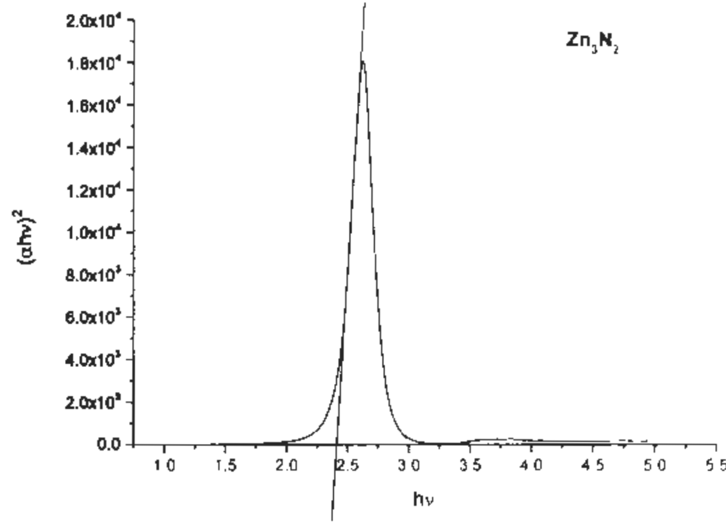

Fig. 4.19: Graph between hv and $(hv\ F(R))^2$ for ZnMg0 $(Zn_{1-x}Mg_x)_3N_2$ (x = 0).

Fig. 4.19 shows the graph plotted between $(hv\ \alpha)^2$ (as F (R) = α) and hv. Thus, the extrapolation of the curve towards hv = 0 gives the band gap value of Zn_3N_2 which is 2.41eV. This increased value is attributed to tensile stresses present in the thin films as already confirmed by the XRD and Raman analysis and presence of ZnO is responsible for this E_g. Moreover, only extrapolated line with a positive slope is considered.

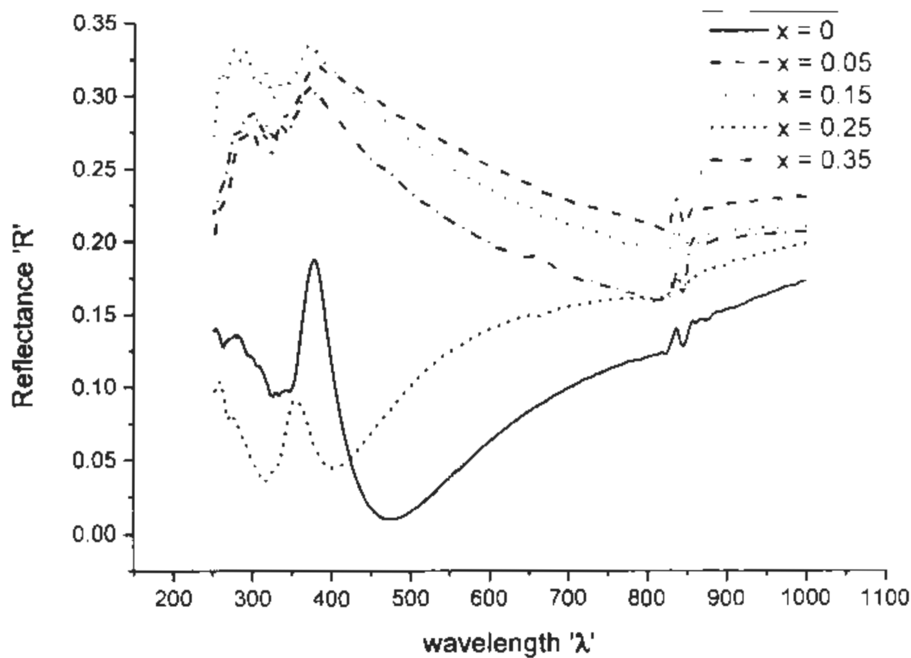

Fig. 4.20: Graph between the wavelength and reflectance of $Zn_{1-x}Mg_x)_3N_2$ with x = 0, 0.05, 0.15, 0.25 & 0.35.

Fig. 4.20 shows the reflectance curves of all the thin film labeled showing which graph belongs to which sample. The figure clearly shows that the curves of ZnMg0 and ZnMg3 are similar to each other. It is evident from XRD as well that ZnMg3 contains less incorporation of Mg may be due to some unintentional ambient conditions' change during fabrication of the thin film. That is the main reason that ZnMg3 has a reflectance curve similar to that of ZnMg0. The band gap of zinc nitride is reported to be mostly in the NIR or IR region of the spectrum [1, 4, 16]. An overall increase in the reflectance of thin films results from the addition of magnesium (i.e. a metal) in the zinc nitride.

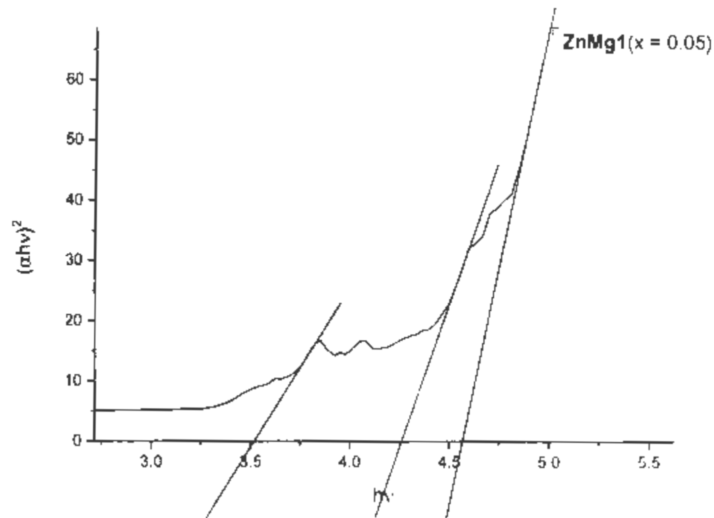

Fig. 4.21: Graph between hv and $(hv\alpha)^2$ for ZnMg1 (x = 0.05).

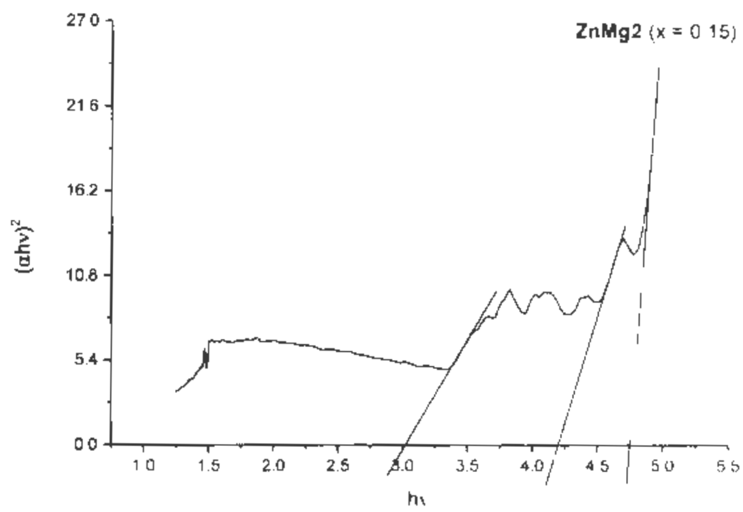

Fig. 4.22: Graph between hv and $(hv\alpha)^2$ for ZnMg2 (x = 0.15).

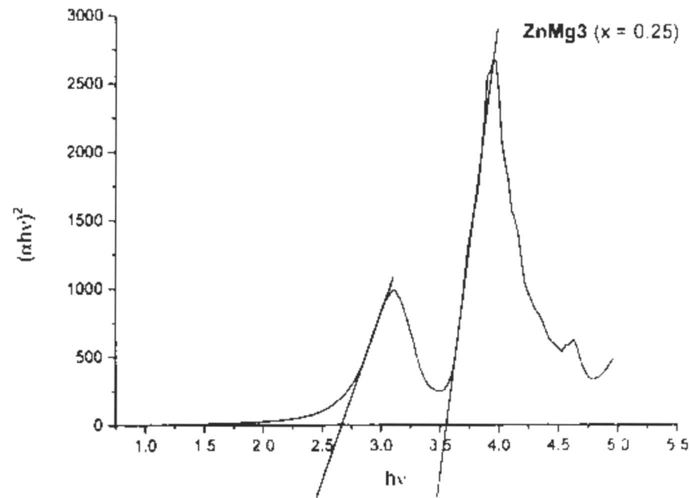

Fig. 4.23: Graph between hv and $(h\nu\alpha)^2$ for ZnMg3 (x = 0.25).

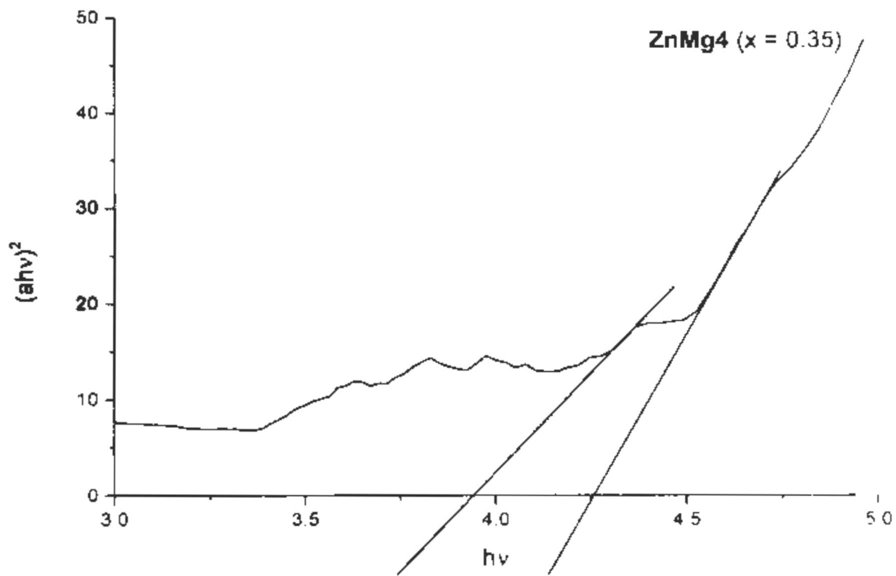

Fig. 4.24: Graph between hv and $(h\nu\alpha)^2$ for ZnMg4 (x = 0.35).

Fig. 4.21, 4.22, 4.23 and 4.24 shows the graph between 'hv' and '$(h\nu\alpha)^2$' for the samples ZnMgl, ZnMg2, ZnMg3 and ZnMg4 respectively. Also, the presence of more than one values of E_g may be attributed to the quantum confinement effect of the thin films. The values of bandgap E_g calculated by the Tauc plot method are given in the table given below:

Samples	E_g values (eV)
Zn_3N_2	2.41
ZnMg1	3.51, 4.26, 4.57
ZnMg2	3.02, 4.19, 4.72
ZnMg3	2.66 & 3.55
ZnMg4	3.94 & 4.26

Table 4.10: E_g values for different thin film samples.

4.4.2 Spectroscopic Ellipsometry:

The main purpose of performing ellipsometry on samples was to find out the approximate thickness of the thin films close to the original value. Many other optical constants can be measured by analyzing and fitting of the ellipsometry data i.e. initial values of the phase and amplitude (φ and Δ) and change in them on getting reflected by the thin film sample. In other words, the change in polarization between the incident and the reflected light. The values that can be calculated by using SE include film thickness, refractive index 'n', extinction coefficient 'k', complex dielectric constant 'ε' etc. It can also give information about the surface roughness, composition, crystallinity, anisotropy, uniformity etc of the thin film samples[46].

Ellipsometry data and its fitting were carried out by using Sentec SE 800 at Advanced Electronics Lab (AEL), IIUI. The model adopted for data fitting was formula Bloomer layer. Mathematical analysis of the ellipsometry data was carried out by using the relation;

$$k = \frac{\alpha\lambda}{4\pi} \quad (4.6)$$

$$\alpha = \frac{4\pi k}{\lambda} \quad (4.7)$$

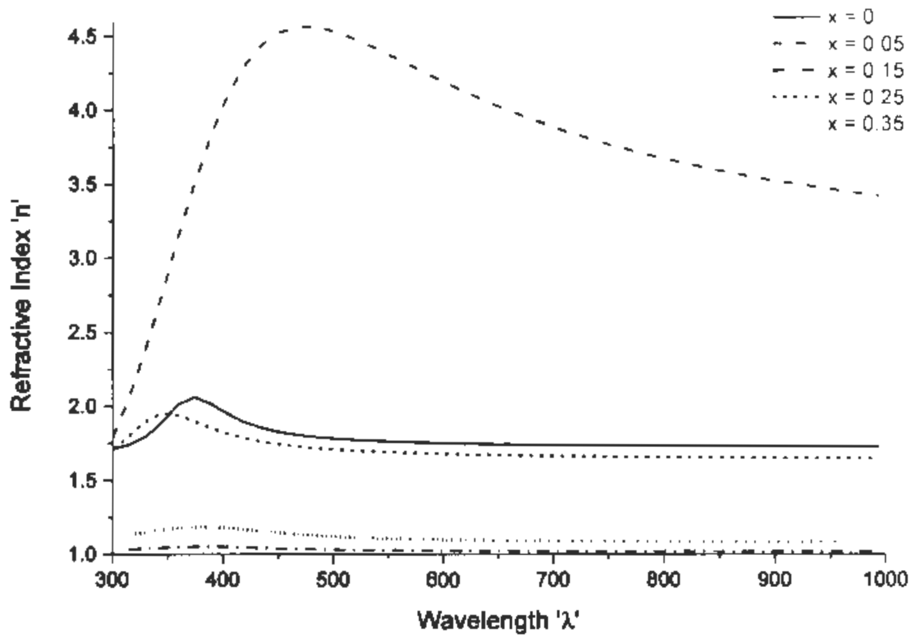

Fig. 4.25: Graph of refractive indices 'n' for $Zn_{1-x}Mg_x)_3N_2$ with x = 0, 0.05, 0.15, 0.25 & 0.35.

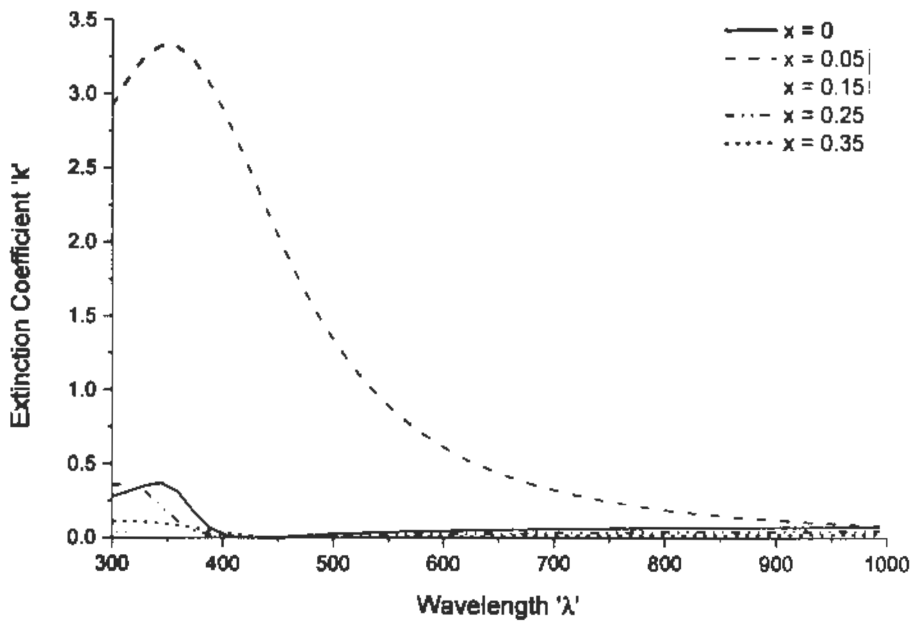

Fig. 4.26: Graph of extinction coefficient 'k' for $Zn_{1-x}Mg_x)_3N_2$ with x = 0, 0.05, 0.15, 0.25 & 0.35.

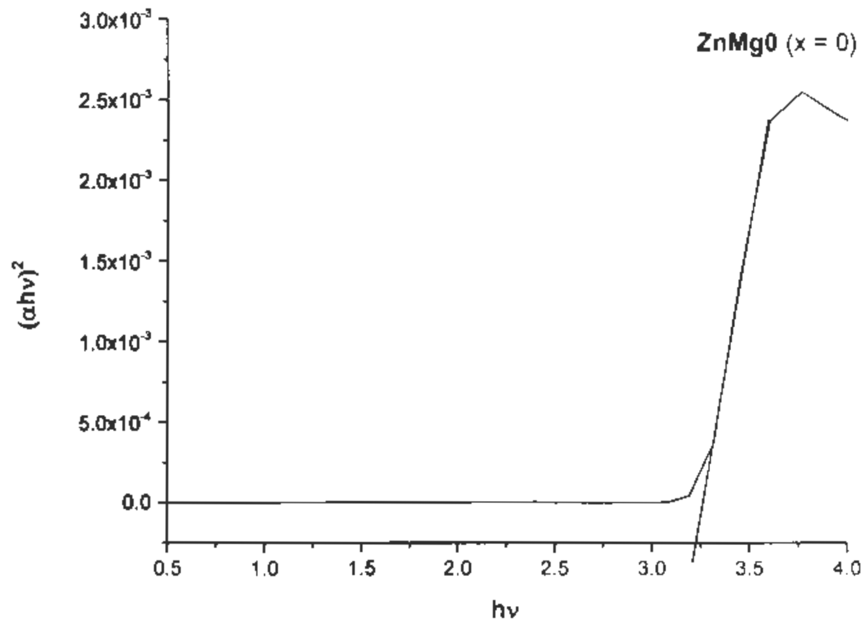

Fig. 4.27: Bandgap calculation of ZnMg0 (x = 0) by SE (using Tauc plot).

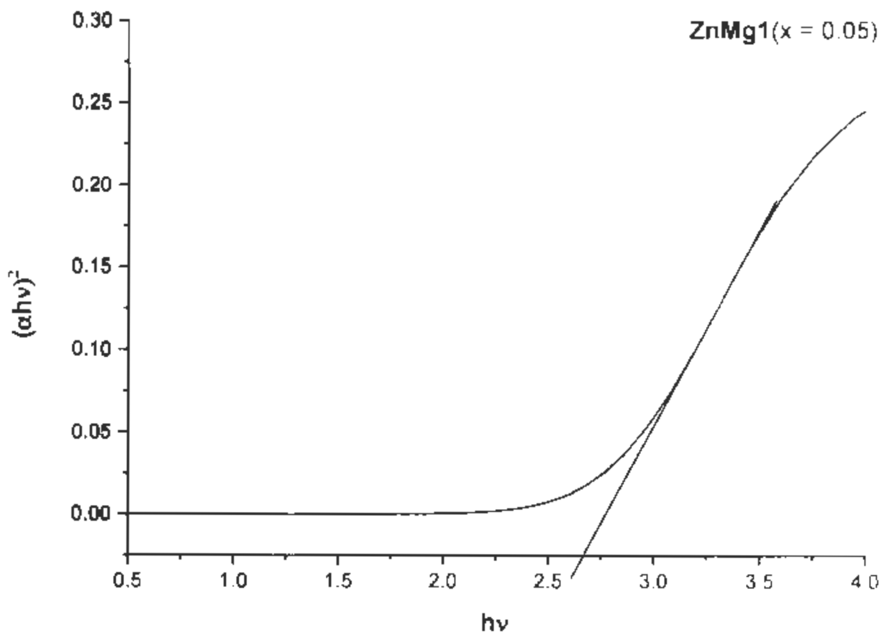

Fig. 4.28: Bandgap calculation of ZnMg1 (x = 0.05) by SE (using Tauc plot).

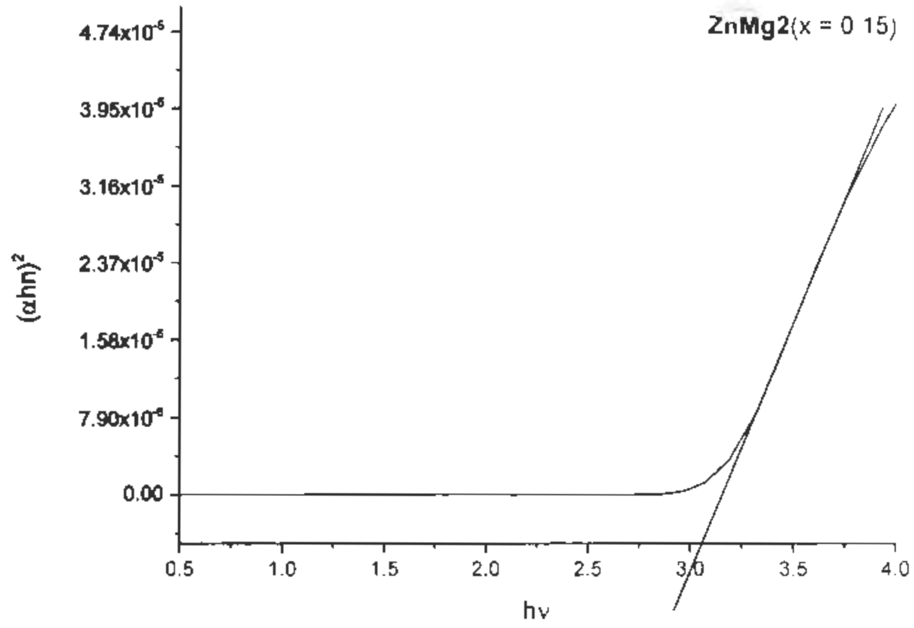

Fig. 4.29: Bandgap calculation of ZnMg2 (x = 0.15) by SE (using Tauc plot).

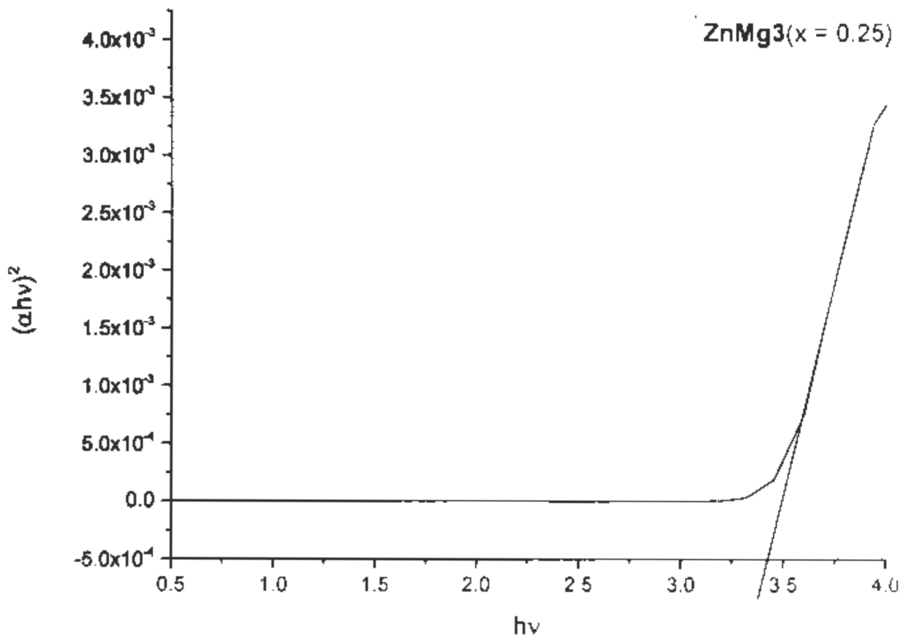

Fig. 4.30: Bandgap calculation of ZnMg3 (x = 0.25) by SE (using Tauc plot).

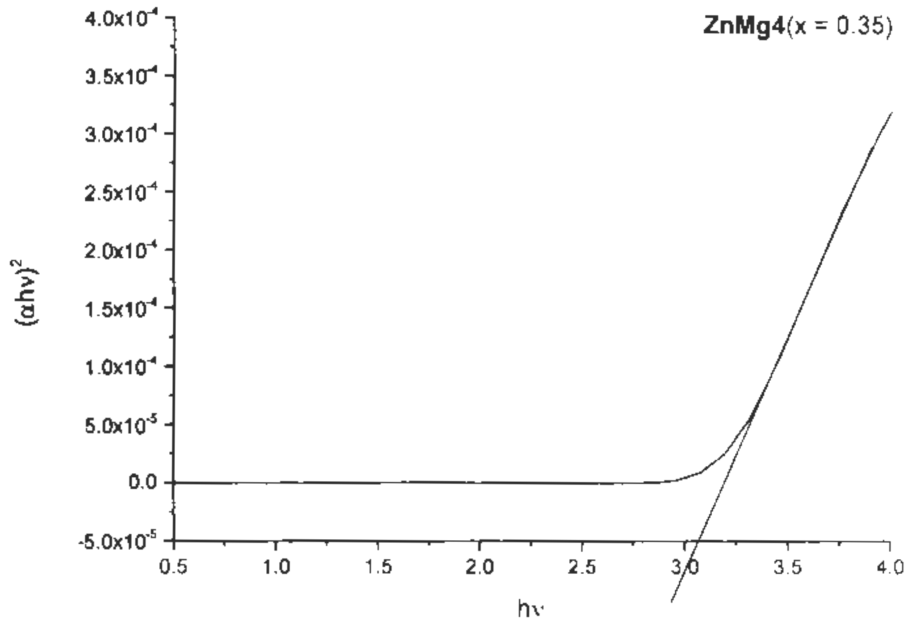

Fig. 4.31: Bandgap calculation of ZnMg4 (x = 0.350 by SE (using Tauc plot).

The values calculated by extrapolating the slope part of the graph between '$(\alpha hv)^2$' and 'hv' are given in the table 4.11 against the samples' names.

Samples	**Bandgap values 'E_g'** (eV)
ZnMg0	3.22
ZnMg1	2.66
ZnMg2	3.06
ZnMg3	3.42
ZnMg4	3.06

Table 4.11: E_g values for different samples calculated by SE.

Table 4.11 shows that values of E_g obtained from SE analysis are not very different from those attained by reflectance analysis.

The values of refractive indices 'n', extinction coefficients 'k' and thin film thickness 't' are stated in the table 4.12 against each sample. In Physics, extinction

coefficient 'k' is the complex part of complex refractive index which also relates to the absorption of light in the thin film.

Samples	**Refractive index 'n'**	**Extinction coefficient 'k'**	**Thin Film Thickness 't' (nm)**
ZnMg0	2.06	1.1×10^{-3}	64.7
ZnMg1	4.57	1.4×10^{-3}	69.76
ZnMg2	1.06	0	105.22
ZnMg3	1.95	1×10^{-4}	49.18
ZnMg4	1.19	1×10^{-4}	61.86

Table 4.12: n & k values for different samples calculated by SE.

Table 4.12 shows the values of 'n' and 'k' calculated for all the thin film samples. The value of n is overall decreasing with increasing the Mg content same as the values of k which became 0 at 15% Mg content.

Samples	**E_g (UV-VIS Ref.) (eV)**	**E_g (Ellipsometry) (eV)**
$(Zn_{1-x}Mg_x)_3N_2$ (x = 0)	2.41	3.22
$(Zn_{1-x}Mg_x)_3N_2$ (x = 0.5)	3.51, 4.26, 4.57	2.66
$(Zn_{1-x}Mg_x)_3N_2$ (x = 0.15)	3.02, 4.19, 4.72	3.02
$(Zn_{1-x}Mg_x)_3N_2$ (x = 0.25)	2.66, 3.55	3.42
$(Zn_{1-x}Mg_x)_3N_2$ (x = 0.35)	3.94, 4.26	3.06

Table 4.13: Comparison of bandgap values calculated by UV-VIS reflectance and SE.

4.5 Conclusions:

- The lattice constant 'a' is increasing with increasing Mg content which proves the incorporation of Mg in the Zn_3N_2 lattice. The micro-strains are positive valued which implies a tensile stresses.
- Raman vibration modes exhibits an overall red shift which shows an increasing bond length.
- Mobility 'μ' is decreasing with increasing number density 'n' which indicates that the impurity scattering mechanism is becoming more and more dominant & crystallinity is decreasing.
- Reflectance is increasing as Mg is increasing as it's a metal.
- SE shows that 'n' & 'k' decreases with increase in Mg content.

****

References:

1. Toyoura, K., et al., *Optical properties of zinc nitride formed by molten salt electrochemical process*. Thin solid films, 2005. **492**(1-2): p. 88-92.
2. Yamada, N., et al., *Transparent conducting zinc nitride films*. Japanese Journal of Applied Physics, 2014. **53**(5S1): p. 05FX01.
3. Juza, H. and Z. Hahn, *Crystal Chemistry of Inorganic Nitrides*. Anorg. Allg. Chem., 1940. **124**: p. 125.
4. Futsuhara, M., K. Yoshioka, and O. Takai, *Structural, electrical and optical properties of zinc nitride thin films prepared by reactive rf magnetron sputtering*. Thin Solid Films, 1998. **322**: p. 274-281.
5. Jiang, N., D.G. Georgiev, and A.H. Jayatissa, *The effects of the pressure and the oxygen content of the sputtering gas on the structure and the properties of zinc oxy-nitride thin films deposited by reactive sputtering of zinc*. Semiconductor Science and Technology, 2013. **28**: p. 025009.
6. Liu, D.-S., C.-S. Sheu, and C.-T. Lee, *Aluminum-nitride codoped zinc oxide films prepared using a radio-frequency magnetron cosputtering system*. Journal of Applied Physics, 2007. **28**(025009): p. 8pp.
7. Gondal, M.A., et al., *Synthesis of ZnO_2 nanoparticles by laser ablation in liquid and their annealing transformation into ZnO nanoparticles*. Applied Surface Science, 2009. **256**: p. 298-304.
8. Kuriyama, K., Y. Takahashi, and F. Sunohara, *Optical band gap of Zn_3N_2 films*. PHYSICAL REVIEW B, 1993. **48**(4): p. 2781-2782.
9. Melo, M.L.L.M.S.d., *Deposition of Zn_3N_2 thin films and application in TFT structures*, in *Physics Dept*. 2014, ist: Lisbon, Portugal.
10. Sinha, S. and S.K. Sarkar, *Atomic layer deposition of textured zinc nitride thin films* RCS Advances, 2014. **4(88)**: p. 47177-47183.
11. Georgiev, D.G., et al., *Microstructure and Electronic Properties of Zinc Nitride Thin Films*, in *Nnaotechnology Materials and Devices Conference*. 2009: Traverse City, Michigan, USA.
12. Yang, T., et al., *Structural and optical properties of zinc nitride films prepared by rf magnetron sputtering*. Applied Surface Science, 2009. **255**: p. 3544-3547.
13. Voulgaropoulou, P., et al., *Optical properties of zinc nitride thin films fabricated by rf-sputtering from ZnN target*. Thin Solid Films, 2008. **516**: p. 8170-8174.
14. Jiang, N., et al., *Zinc nitride films prepared by reactive RF magnetron sputtering of zinc in nitrogen containing atmosphere*. Journal of Physics D: Applied Physics, 2012. **45**(135101): p. 9pp.
15. Xing, G.Z., et al., *Structural and electrical characteristics of high quality (100) orientated- Zn_3N_2 thin films grown by radio-frequency magnetron sputtering*. Journal of Applied Physics, 2010. **108**: p. 083710.
16. Ebru, S.T., K. Hamide, and E. Ramazan, *Structural and optical properties of zinc nitride films prepared by pulsed filtered cathodic vacuum arc deposition*. Chin. Phys. Lett., 2007. **24**(12): p. 3477-3480.
17. Suda, T. and K. Kakishita, *Band-gap energy and electron effective mass of polycrystalline Zn_3N_2*. Journal of Applied Physics, 2006. **99**(7): p. 076101.

18. Kambilafka, V., et al., *The effect of nitrogen on the properties of zinc nitride thin films and their conversion into p-ZnO:N films.* Thin Solid Films, 2007. **515**(24): p. 8573-8576.
19. Kambilafka, V., et al., *Thermal oxidation of n-type ZnN films made by rf-sputtering from a zinc nitride target, and their conversion into p-type films* Superlattices and Microstructures, 2007. **42**: p. 55-61.
20. *static.ifp.tuwien.ac.at/homepages/Personen/Thin film technology/Physics of thin films.* .
21. *https://en.wikipedia.org/wiki/Epitaxy.*
22. Khan, S., *Deposition of silicon nitride film by dc reactive magnetron sputtering*, in *Department of DCME.* 2008, Pakistan Institute of Engineering and Applied Sciences: Islamabad, Pakistan.
23. Krebs, H.-U., et al., *Pulsed Laser Deposition (PLD) - a Versatile Thin Film Technique.* Advances in Solid State Physics, 2003. **43**: p. 14.
24. Hayat, A., *Growth and characterization of $Zn_{(1-x)}Mg_xO$ thin films used for UV photodetectors.* 2008, COMSATS Islamabad.
25. Ebrahimi, M., *Atomic Layer Deposition (ALD).* 2006, University of Waterloo.
26. Rashid, R., *Synthesis and characterization of TiO_2-Ge thin films for photovoltaic application*, in *Physics Dep.* 2009, Pakistan Institute of Engineering and Applied Sciences (PIEAS): Islamabad, Pakistan.
27. Choi, C.-H. and S.-H. Kim, *Effects of post-annealing temperature on structural, optical, and electrical properties of ZnO and $Zn_{1-x}Mg_xO$ films by reactive RF magnetron sputtering.* Journal of Crystal Growth, 2005. **283**: p. 170-179.
28. Ye, Z.-Z., et al., *Preparation and characteristics of p-type ZnO films by DC reactive magnetron sputtering.* Journal of Crystal Growth, 2003. **253**: p. 258-264.
29. Sharma, S., et al., *Structural and optical characterization of ZnO thin films for optoelectronic device applications by RF sputtering technique.* Superlattices and Microstructures, 2014. **75**: p. 378-389.
30. Hamid, H.B.A., *Fabrication, structural and electrical characteristics of Zinc Oxide (ZnO) thin films by DC sputtering.* 2009, Universiti sains Malaysia.
31. Kirschbrown, J. (2007) *RF /DC Magnetron Sputtering.*
32. Kirschbrown, J., *RF /DC Magnetron Sputtering.* 2007.
33. *www.slideserve.com/raleigh/sputtering.*
34. Liu, Y., Y. Li, and H. Zeng, *ZnO-Based Transparent Conductive Thin Films Doping, performance and processing* Journal of Nanomaterials, 2013.
35. Kaur, R., *Magnetic behaviour of Co doped CdSe nanoparticles as dilute magnetic semiconductor.*, in *School of Physics and Materials Science* 2012, Thapar University: Patiala.
36. Jalili, N. and K. Laxminarayana, *A review of atomic force microscopy imaging systems "Application to molecular metrology and biological sciences"* Int Journal of Material Characterization, 2004. **14**: p. 907-945.
37. *Academic.brooklyn.cuny.edu/physics/holden/ellipsometry htm.*
38. Martinez, J.C., et al., *Alternative Methodology for Gold Nanoparticles Diameter Characterization Using PCA Technique and UV-VIS Spectrophotometry.* Nanoscience and Nanotechnology, 2012. **2**(6): p. 184-189
39. *http://www.ece.gatech.edu/research/labs/vc/theory/sheetRes.html.*
40. Pauw, L.J.v.d., *A method of measuring the resistivity and Hall coefficient of lamellie of arbitrary shape.* Philips Technical Review. **20**(8): p. 220-224.

41. http://pd.chem.ucl.ac.uk/pdnn/peaks/size.htm.
42. Wang, X.H., et al., *Optical properties of p-type ZnO doped by lithium and nitrogen*. Solid State Communications, 2007. **141**: p. 600-604.
43. Singh, S. and p. Chakrabarti, *Comparison of the structural and optical properties of ZnO thin films deposited by three different methods for optoelectronic applications*. Superlattices and Microstructures, 2013. **64**: p. 283-293.
44. Erdogan, N.H., et al., *Effect of the oxidation temperature on microstructure and conductivity of Zn_xN_y thin films and their conversion into p-type ZnO:N films*. Applied Surface Science, 2013. **271**: p. 70-76.
45. Jafarkhani, P., et al., *Synthesis of nanocrystalline titania in pure water by pulsed Nd:YAG Laser*. Applied Surface Science, 2010. **256**(12): p. 3817-3821.
46. *https://en.wikipedia.org/wiki/Ellipsometry*.